Simple holistic solution to Archie's-law puzzle in porous media

Isaac Balberg*
The Racah Institute of Physics, The Hebrew University, Jerusalem 9190401, Israel

(Received 11 February 2021; accepted 21 May 2021; published 21 June 2021)

In this paper, we account for the many critical exponents derived from the studies of the electrical conductivity in porous media by applying analysis of the well-known relation known as Archie's law. In spite of its seeming simplicity this law is considered to be "poorly understood," and the question that was and still is debated in the literature is whether there is some "hidden physics" in this law, or if it is "strictly a parametrization use for curve fitting with *a priori* no physical meaning." Our solution to the corresponding long-debated 78 years old puzzle is based on the classical percolation theory, but it also involves a principle that is based on continuum percolation. This principle is that the electrical properties of a percolation system are determined by the interplay between the connectivity of the conducting objects in that system, and the connectivity of the intersections between pairs of them. We thus propose a general concept that we call an electrically affected connectivity, and we predict the corresponding evolvement of the conductivity critical exponent with the increase of the content of the electrically conducting phase. Then, we show that the zerolike threshold that characterizes Archie's law is what enables the observation of this evolution. Combining the above principle and the latter feature, we provide a holistic, yet simple, solution to the longstanding controversy surrounding this law and its practical applications. In contrast with many previous claims that Archie's law lacks a physical basis, and the commonly suggested experiential explanations for it, we provide a solution that is physically based and thus elucidates Archie's law by showing clearly that it represents a bona fide phase transition phenomenon. This conclusion and its generality are strongly supported by the fact that it also explains the behavior of the electrical conductivity exponents in nonporous systems such as composite materials. The predicted ability to extract the long sought microgeometrical information from Archie's-law data, within the framework of the percolation phase transition, is expected to open a new direction in the understanding and the applications of this law.

DOI: 10.1103/PhysRevE.103.063005

I. INTRODUCTION

Since Archie's seminal realization [1] regarding the dependence of electrical conductivity in porous media on the porosity ϕ (the fractional macroscopic volume of the pores), 78 years ago, this dependence has been a subject of great interest due to its relevance for many science and engineering fields. The dependence, known as Archie's law states that in many porous media, when saturated with an electrically conducting liquid (typically water or brine), the electrical conductivity σ is simply given by $\sigma \propto \phi^m$, where m is an empirical parameter. Though Archie proposed this dependence for sedimentary rocks, such as sandstones (for which he found an $m \approx 2.0$ value) and unconsolidated sand (for which he found an $m = 1.3$ value), it was later widely applied to other fields [2–8], including physics [3,9,10], statistical physics [11,12], material science [13–17] and engineering [18], as well as mathematics, statistics, and computer science. In particular, *to this very day,* Archie's law is used extensively for understanding, system-characterization [19], and the extraction of valuable information [5] in earth sciences, including geophysics [20,21], geology [6,22], hydrology [23,24], agriculture [20,25], petrophysics [5,26,27], mineralogy [28,29], seismology [30–32], and many environmental sciences [33–35]. In fact, due to the abundance of its observation "this empirical relation has been accorded the status of a law in the geophysical literature" [2] and a distinction was made between Archie's [36] and non-Archie's [37] rocks.

The two conspicuous features of Archie's "law" [1], when it is written as

$$\sigma \propto (\phi - \phi_c)^m, \tag{1}$$

are that ϕ_c, the threshold porosity for electrical conductivity, is practically 0 [1,3], and that the exponent m, as determined in numerous observations, is confined to well-defined ranges; these are the $2.0 \leqslant m \leqslant 4.0$ range [4,38,39], the $1.3 \leqslant m \leqslant 2.6$ range [40–42], the $1.0 \leqslant m \leqslant 1.3$ range [43], and the $1.0 \leqslant m \leqslant 2.0$ [6] range. Archie attributed the m values that he found to the cementation in sedimentary rocks, and thus m is also known as the cementation factor [44]. In spite of its simplicity the interpretation of this law has created a lively ongoing controversy [2,19,40,45,46] that continues until today [39,47–52]. Correspondingly, the law is still described as "poorly understood" [36] or "inadequately understood" [48]. While numerous various approaches and ad hoc models for the explanation of the various m values in the above m ranges were suggested [5,37,41,42], some very significant characteristics of these values have not been accounted for. These include the sharp statistical drop in the number of

*balberg@mail.huji.ac .il

observations beyond $m = 4.0$ [38,53], the frequent observations of a series of m values in a given reservoir in the $1.3 \leqslant m \leqslant 2.6$ range for very different types of reservoirs [40,41,54], and the observed increase [22,40,44,53] or decrease [19,22,40,41,53] of the $m(\phi)$ dependencies. More significantly, none of the previously proposed models [39,55] was able to give a general and holistic account that correlates Archie's m confinements with Archie's $\phi_c \to 0$ feature. For more of the observed m values see the Supplemental Material SM(1) in Ref. [56].

The many trials to interpret this law in terms of percolation theory have faced two major difficulties. First, it is counterintuitive to have an electrical conductivity threshold, ϕ_c, that is zero [41,70], and second, *no previous percolation model could explain the general confinement of the m values to the* $1.0 \leqslant m \leqslant 4.0$ *range* [2,38,39,43,44,53]. Moreover, the significant similarity of the above observations to those found in (the physically very different, but topologically very similar) composite materials [71–73] *has not been noticed*. On the other hand, the frequent experimental observations [1,2,38] of 1.3 and 2.0 values of m in porous media, and the corresponding conductivity exponent in composite materials, indicate the relevance of percolation theory since these values are the two dimensional, $\mu(2D)$, and the three-dimensional, $\mu(3D)$, percolation universal-critical exponents of the percolation conductivity [74–76]. Below, we denote these two exponents generically by μ (see SM(2) in Ref. [56]). In contrast with the latter μ values, m values larger than $m = 2.5$ in various porous media [70,77] cannot be explained even by the well-known possible deviations from percolation universality [2,78] (see SM(3) in Ref. [56]), or by uncommon percolation theories [9]. In particular, no previous percolation approach could account for the above-mentioned sharp statistical drop in the observations of the m values for $m > 4.0$. Correspondingly, the above variety of m values [2,19,38,54] and the *a priori* unphysical [41,54,70] finding [1,3] of $\phi_c \to 0$, have motivated many [2,19,36] to interpret the observations of Archie's law outside the common framework of percolation theory [39,41,42,54]. In fact, the observation of m values in the $1.5 \leqslant m \leqslant 2.2$ range, on a particular type of microstructure, has been interpreted as evidence that such observations "mediate against percolation models as suitable models of rock pore-space geometry" [41]. Still, following the overwhelming finding of $m = \mu$ values in a variety of the studied porous media [2,19], many others tried to interpret Archie's law [2,3,79] in light of the first principles of percolation theory [74–76,78] (see SM(2) in Ref. [56]).

In this paper, we add to our previous percolation explanation of Archie's $\phi_c \to 0$ feature [3], a simple percolation-based analysis that accounts for the various observations concerning the m value confinements and the $m(\phi)$ dependencies in porous media. This is done by showing that those confinements result when the electrical resistance at the intersection between two pores, that are saturated with a conducting liquid, is larger than that of the corresponding individual pores, and by showing that the observation of these confinements is enabled by the $\phi_c \to 0$ feature. Such conditions commonly exist in systems of slender (i.e., high aspect ratio) pores, where the pores have the form of channels [4,5], fractures [3,6], and cracks [80,81], or narrow throats that connect spherical-like pores [2,36,54]. In particular, we show that the smaller the ϕ_c, the larger the probability for observing m values in the interval $1.3 \leqslant m \leqslant 2.6$ in two-dimensional systems, and in the interval $2.0 \leqslant m \leqslant 4.0$ in three-dimensional systems. Proving the relation between the observed confinement of the m values and the $\phi_c \to 0$ threshold provides then *a holistic solution to the puzzle that accompanies the numerous observations of Archie's law*. Our study presents then a significant advance in the field, the state of which is clearly reflected in recent statements such as "there is no universal model that simultaneously captures the physical characteristic of all porous media" [39], or that "the physical basis of Archie's law has not been fully understood yet" [11]. The fact that our model can explain similar confinements in composite materials [71] further shows that, in contrast with suggestions that "there is no physics to be found in Archie's m" [36] and that it lacks "support from first principles" [7], our present interpretation rests on the firmly based theory of continuum percolation as a phase transition [78]. Moreover, in contrast to the attribution of the m values to a nonspecific "variety of factors" [38,54], and the conclusion that while m "must contain" information on brine geometry it is not in a "readily interpretable form" [36], we are able to show that there are global-system parameters that determine the $m(\phi)$ values and connect them to that geometry. The present work then finally enables us to overturn the claims that the "physical basis for Archie's law still remains a debated question" [8] and that "at present there is no consensus on the physical meaning of m" [11].

This paper is organized as follows. In Sec. II we briefly review the solution that we provided in Ref. [3] to the first conspicuous feature of Archie's law, i.e., the $\phi_c \to 0$ threshold. However, in order to show that our conclusions in the present work are universal, we also prove that our arguments there apply not only to porous media but also to the topologically similar group of composite materials. Then, in Sec. III, we turn to the main subject of our present work, which is the solution to the second conspicuous feature of Archie's law, i.e., the basic physics explanation of the numerous $m(\phi)$ values and the reason for their confinements as observed in various types of porous media. In Sec. IV, we show that our predictions are well supported by experimental and computational observations and we discuss the significant progress that we have made here beyond the previous understanding of Archie's law. Finally, in Sec. V we summarize our main conclusions and the research and application directions that they suggest.

II. THE SOLUTION TO ARCHIE'S NEAR-ZERO THRESHOLD PROBLEM

Our account of the near-zero porosity threshold of Archie's law (presented in Ref. [3]) is based on the concept of the excluded volume [82], and is as follows. The average excluded volume V_{ex} of a convex permeable (or "soft core" [73,78]) object that has a volume V, is the volume in which the center of another similar convex object must be in order for them to intersect. The objects that intersect, and thus partially overlap, are defined as connected. For the simple 2D line-segment systems that are illustrated in Fig. 1, the excluded area of a line segment A_{ex} is given by $\langle L^2 \rangle \langle \sin\theta \rangle$. Here, L is a length of a segment ($\langle L^2 \rangle$ is the proper average of L^2) and θ is

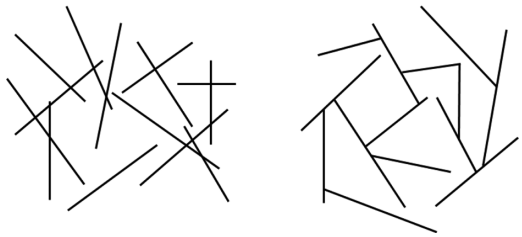

FIG. 1. Small portions of 2D line-segment systems that represent ensembles of channels in porous media. The line segments here have an average length L and an average width δ (such that $L \gg \delta$). The system on the left is known as having the 2D "face-face" configuration and the system on the right is known as having the 2D "vertex-face" configuration [88,89]. In particular, these line-segment systems can represent an aerial image of a ranch of fractures or a fault zone [80] as well as the intersections of the fracture planes with the ground surface [90]. If these planes are perpendicular to the ground surface, their corresponding ensembles are 2D percolation systems, while otherwise, the systems in the figure reflect 3D percolation systems [3,91]. Similarly, these line segments represent a 2D projection of conducting nanotubes that are embedded in their polymer composite [71,73,92]. For systems that contain permeable objects, such as pores, if they are slender as in the figure, the volume of an intersection is very small compared to the object's volume V and thus $\phi \approx n_f V$ [93], where n_f is the concentration of the conducting objects. In all those systems, each conducting object may have an average resistance r_f and each intersection between two objects may have an average resistance r_i. Once n_f is higher than the percolation threshold n_{fc}, if $r_f \gg r_i$, the global conductivity σ is proportional to $1/r_f$ [87], while if $r_i \gg r_f$, σ is proportional to $1/r_i$ [86]. A translation of the geometrical system, that is shown on the left of the figure, to an electrical resistors network, is described in Ref. [86].

the angle between two intersecting segments. For example, in the corresponding isotropic case (i.e., when $-\pi/2 \leqslant \theta \leqslant \pi/2$), $\langle \sin\theta \rangle = 2/\pi$ [82]. As shown previously, similar A_{ex} expressions can describe porous media that contain permeable slender pores, such as ensembles of channels [4,5], cracks [80,81,83], or fractures [3,6,84,85]. Correspondingly, the line-segment models of Fig. 1 are used throughout this paper as simple representations of those systems. When the pores in porous media are saturated with a conducting fluid, they provide electrical networks in which the conducting elements, i.e., the filled pores, have an average electrical resistance r_f and their intersections have an average electrical resistance r_i. In all the above systems, when the concentration of the conducting elements, n_f, reaches a critical value n_{fc}, there will be an onset of a macroscopic geometrical and electrical connectivity. For permeable line-segment systems, such as in Fig. 1, we have previously demonstrated a percolation universal-critical [i.e., an $m = \mu(2D)$] behavior, by a simulation for the $r_i \gg r_f$ case [86], and by a computer-driven experiment, for the $r_f \gg r_i$ case [87].

To make our 2D "face-face" model of Fig. 1 tangible for systems of fractures and their intersections in 3D porous media, we illustrate in Fig. 2 two polygons that represent two conducting liquid-saturated fractures and their subsequent intersection. Here we note that there are quite a few scenarios of fracture intersections [88].

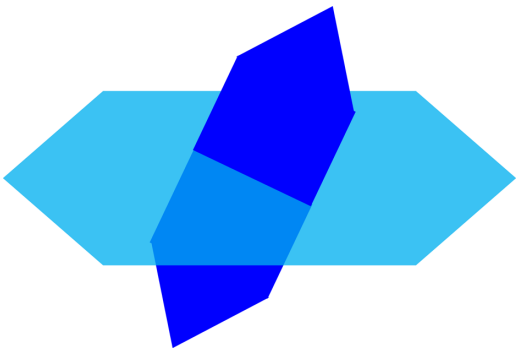

FIG. 2. A 3D illustration of an intersection of two polygons that represent two brine-saturated fractures in the "face-face" configuration [88]. The electrical current that passes from one fracture to another (each of resistance r_f) must cross through their intersection junction which has a resistance r_i.

In general, the average number of permeable objects that intersect a given object (here a line segment or a polygon), i.e., the number of objects' centers within the excluded area or excluded volume of an adjacent object, is $B = n_f A_{ex}$ or $B = n_f V_{ex}$. Thus, a global geometrical connectivity will result when B (i.e., n_f) reaches the corresponding topologically required threshold value $B = B_c$ [94]. The percolation threshold in continuum systems n_{fc} is given then, simply, by $n_{fc} = B_c/A_{ex}$ or $n_{fc} = B_c/V_{ex}$ [82].

Now let us consider the 2D and 3D percolation thresholds in systems of permeable slender objects, i.e., objects with an extreme, $L \gg \delta$, aspect ratio. In the 2D line-segment models of Fig. 1 the average area of the intersections per slender object is on the order of $B\langle\delta^2\rangle$, which is much smaller than the average area of the line segment itself A (here $\langle L\delta \rangle$), and thus one can approximate the corresponding 2D porosity ϕ by $n_f A$. Considering the above $A_{ex} = \langle L^2 \rangle \langle \sin\theta \rangle$ relation, the fractional covered area of these slender objects at the percolation threshold is closely approximated then by [82] $\phi_c \approx n_{fc} A = B_c A/A_{ex}$ i.e., $\phi_c \propto \langle L\delta \rangle / \langle L^2 \rangle$. We have previously generalized this argument to various 2D and 3D systems [3,94] concluding that it applies to any system of slender pores where L represents the large geometrical feature and δ represents the small geometrical feature of the pores. In particular, we can consider a fracture or a crack [85,88,95] in 3D as a 2D polygon of L-long edges and aperture δ, or a disk of radius L and a thickness $\delta(\ll L)$. This yields that, for the isotropic distribution of the orientations of the slender objects, $\phi_c = c\langle L\delta \rangle / \langle L^2 \rangle$ with $c \approx 6$ in 2D, and $\phi_c = c\langle L^2\delta \rangle / \langle L^3 \rangle$ with $c \approx 2$ in 3D [3]. The important point to notice here is that in most of the corresponding natural porous media, the 2D, $\langle L\delta \rangle / \langle L^2 \rangle$, ratio, and the 3D, $\langle L^2\delta \rangle / \langle L^3 \rangle$, ratio are on the order of 10^{-2}. Hence, within the limited accuracy of the available measurements on porous media [47], one cannot clearly establish that the derived ϕ_c values are actually different from zero. We thus concluded [3] that the reason for the "observed" $\phi_c = 0$-like threshold in Archie's law is simply a matter of experimental limitation. In passing, we remark that this feature was considered by some [9] to be a genuine $\phi_c = 0$ result in spite of the apparent counterintuitive nature of such a suggestion [54,70].

The similarity that we have noticed above between the electrical conductivity behavior of porous media and composite materials (see SM(1) in Ref. [56]) calls for a brief comparison of the percolation thresholds in those systems when the conducting objects in them are slender. We start by noting that the objects in composites are nonpermeable particles with volume V each, and their concentration is n_f. Then we note that in all systems of nonpermeable particles, the fractional volume of the conducting phase in the system x is simply given by $x = n_f V$ [38,96], and thus, the percolation conductivity dependence on it is given by [71,93]

$$\sigma \propto (x - x_c)^t, \tag{2}$$

where x_c is the threshold value for the onset of conductivity and t is the experimentally or computationally derived exponent. For composite materials in which the conducting particles are slender (such as in composites of metallic wires embedded in a polymer [72]), we have shown [73] that the above $V_{ex} \gg V$ property yields the same relations that we found for porous media with permeable slender pores. In particular, we found that, as in the above-described porous media, the percolation threshold is very small ($x_c \ll 1$). Indeed, those $x_c \to 0$ results were found [97,98] in many composites with slender conducting particles (in particular when such particles are somewhat elastically bendable [73]). These include, for example, polymer composites with disklike graphene particles [73] (as in fracturelike pores) or carbon nanotubes (CNTs) and metal nanowires [72,73,93] (as in channel-like pores). Hence, systems such as in Fig. 1 have been used by us [73] and by many others [92,99,100] as representative models of those composites. Here we note, however, that unlike the limited experimental resolution in the determination of very small ϕ values in porous media (in particular in natural samples [47,81]), extremely small x values, as small as $x \approx 10^{-5}$, have been controlled and/or monitored in composite materials [97,98]. This can explain well why, in contrast with the evaluation of the finite x_c values in composite materials, the evaluation of ϕ_c values, as small as $\phi \leqslant 10^{-2}$ in porous media, were taken by Archie [1] and some later researchers [9] as implying that $\phi_c = 0$. Following the above, we apply throughout this work the conclusion that very small percolation thresholds will be induced in systems of conducting slender objects, whether they are permeable or not.

III. THE SOLUTION TO ARCHIE'S-EXPONENT PROBLEM

A. Conductivity exponent values as observed in systems of conducting slender objects

Turning to the present, more difficult, issue of the m values that were derived in numerous studies by fitting experimental data [2,19,38,39] to Archie's law, as given by Eq. (1) with $\phi_c = 0$, we consider first the similarity between those m values and the results that have been obtained on the physically quite different composite materials [71,72,98]. Thus far, this similarity has gone unnoticed. As mentioned in Sec. II, for many of the latter types of composites that contain slender nonpermeable conducting particles, we have already shown [73] that the percolation threshold of conductivity can be fully accounted for by considering those particles as slender permeablelike conducting objects. Thus, topologically, such composites resemble porous media where the conducting objects are pore channels [4,87] or pore fractures [3,6] embedded in a rock. During the present work, we have further noticed that just as for the m values in porous media [38–40], the t values of Eq. (2) in those composites have also been found to be confined to the 1.3–4.0 interval [71] and/or the 1.3–2.6 subinterval [71,72]. In particular, we have recognized that many simulations of 2D systems of conducting fibers, where one is certain that no nonuniversal effects (see SM(3) in Ref. [56]) are present, have shown, as do the $m(\phi)$ values in porous media, an increasing $t(x)$ (>1.3) dependence with the departure of x from x_c [72,92,99,100]. Those exact same behaviors of the m and t values suggested to us that there must be some underlying common basic physical-universal principle that has to do with a so far unraveled *connectivity-conductivity* relation in continuum percolation. Further below we suggest such a relationship and apply it for a holistic solution to the puzzle [54] associated with the $\phi_c \to 0$ and the m values that characterize Archie's law.

For simplicity and transparency of our determination of the m and t values in systems of conducting slender objects, we consider the very simple model of the 2D line-segment systems that are illustrated in Fig. 1. As mentioned above, such a model [87] is widely used to represent an aerial view of a "fracture farm" [8,80] or a network of channels [4,84] in porous media, as well as ensembles of CNTs [73,92,99,100] or metallic nanowires [72] in composites. In fact, it is important to emphasize that the models illustrated in Fig. 1 are not just illustrative-abstract ones, but they can be actual presentations of 2D and 3D real systems. For example, an aerial photograph of the Yosemite creek basin north of Yosemite valley [90] resembles the systems shown in Fig. 1, not only geometrically, but also "physically." This is in the sense that the segments in that photograph are the marks of the vegetation growth that results from water filling the fractures in the rock. Hence, the line-segment model provides an appropriate representation of water-saturated geological cracks or fracture plains and their mutual intersections. Correspondingly, *our following conclusions that are based on the line-segment model can be generalized to other types of porous media where the conducting pore elements are slender*. In particular, these include the intersections in systems of channels [4,5], disklike fractures [3,4,6,84], and geological cracks [80,81]. Such are "face-face" (X-like) plain intersections [84,88] and "vertex-face" (T-like) plain intersections [88,89].

In our adoption of the model of Fig. 1 to describe the electrical properties of slender pores and their intersections in porous media, we assume that each line segment (or part of it between subsequent intersections) represents a brine-filled pore that has (on the average of all participating pores) a resistance r_f. Similarly, we assume that each intersection of two pores represents a resistor with an ensemble-average resistance r_i. The global conductivity of the system may be determined then by the resistance of the pores, the resistance of their intersections, or by a combination of both. As our solution to Archie's puzzle is largely associated with the frequently observed $r_i \gg r_f$ scenario, we briefly describe now porous media in which such a scenario can come about.

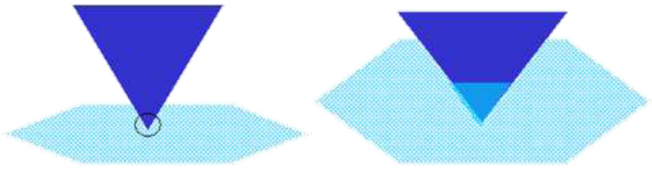

FIG. 3. An illustration of two of the possible 3D configurations of fracture intersections: a "vertex-face" (or a T-like) type [88,89] (left), and a "face-face" (or an X-like) type [84,88] (right). In the corresponding series of resistors, the resistance associated with the intersection junction is $r_f + r_i + r_f$. When $r_i \gg r_f$, this yields a bottleneck effect due to r_i. Apart from geometrical considerations, other factors can further enhance the resistance of the intersections. For example, the X-like and T-like intersections are well known to be narrowed by various clogging effects in them [5,84].

B. Porous media configurations in which $r_i \gg r_f$

Considering the richness of geological-hydraulic systems in general, and the abundance of media with high-resistance bottlenecks in particular, it is not too surprising that many types of porous media exist in which $r_i \gg r_f$. This abundance can be the result of a variety of geometrical and/or physical factors. To introduce such systems, we turn from our 2D line-segment models of Fig. 1 to their 3D equivalents in porous media. In Fig. 3 we illustrate, then, two configurations of plain triangles that represent slender pores that are saturated with a stationary electrically conducting liquid and their intersections. We note of course that when modeling such systems, the values of r_f and r_i are statistical averages of the corresponding pores' resistances and the pore-intersections' resistances, respectively. Hence, in continuum systems in general and in porous media in particular, the r_i/r_f ratio is the culminated resultant of these two averages.

For brevity, we narrow our discussion to just a few representative examples of the many relevant pore configurations [45,46,70,77,88,91,101,102] that arise in porous media formations. A simple way to appreciate a geometrically induced $r_i \gg r_f$ scenario is to consider two fractures of size L^2 and aperture W, and the intersection between them [88]. Of the corresponding intersections' configurations, the simplest and most abundant ones are the "vertex-face" (left) and the "face-face" (right) types that are illustrated in Fig. 3. The electrical properties of the first configuration can be understood by applying the analysis of the "point contact" between a sharp metallic tip and a semiconductor surface that causes an electrical junction of high resistance (which is inversely proportional to the radius of the contact [103,104]). In that configuration, if the vertex is assumed to be a tip of radius $\varepsilon \ll W$, the resistance of this intersection penetration is proportional then to $1/\varepsilon$, and thus, for these configurations, for $\varepsilon \ll W$, we have that $r_i/r_f \approx W/\varepsilon \gg 1$. A related configuration that can yield an $r_i \gg r_f$ relation in the intersection of two fractures is their "edge-edge" configuration in which the lines of the edges are at a finite angle with each other [88]. In this configuration, the fractures can be represented by parallelepipeds of size L^2 and aperture W, and the edges of the fractures can be assumed, for simplicity, to be half cylinders with a radius $W/2$. The corresponding (sphere-sphere like) intersection can be described then by half-cylinder overlap with a depth ε. In this case, the resistance of this intersection, for $W \gg \varepsilon$ and brine resistivity ρ, is $r_i \approx (2/\pi)\rho/(\varepsilon W)^{1/2}$ [91] while $r_f \approx \rho/W$. Thus, the $r_i/r_f \approx (W/\varepsilon)^{1/2}$ ratio can yield an $r_i/r_f \gg 1$ scenario.

The other "face-face" [88] (or X-like [84]) configuration [88], which is probably more abundant, is that of two conducting (liquid-filled) planelike fractures that, as illustrated in Fig. 3, have a penetrating intersection with each other. In that, as well as in other configurations, one finds various intersection-damage zones that can cause a significant narrowing of the effective electrical contact cross section between the intersecting fractures [105]. Another well-known narrowing effect of the intersection is due to a "mass accumulation" [102], such as solute deposition [84] and/or bioclogging [2]. These reductions of the cross section at the intersections (as in the case of T [89] or X [88] connections of pipes) are due to the slowing of the fluid flow at the intersections during the rock formation diagenesis [106]. Similarly, the compaction of the system due to external pressures can cause further narrowing of the cross sections for electrical current at the intersections [11]. Another reason for high resistance at the intersections may be of chemical origin, e.g., various mineral drainage products [84,106] that cause differences in salinization in the fracture and the intersection which can yield a further enhancement of the r_i/r_f ratio. We must emphasize, however, that throughout this work we are concerned with electrical conductivity observations in the porous medium after the completion of its geological-hydraulic formation processes. The implicit assumption here is that, as in the commonly discussed Archie's-law systems [39], the pores are saturated with a stationary liquid, i.e., the liquid does not flow in the system during the measurement of the electrical conductivity.

It is quite important here to recall the analogy between the above described high r_i/r_f ratios in porous media and the high r_i/r_f ratio in composite materials. In the latter systems, the "intersection" [73] between adjacent nonpermeable particles (with a resistance r_f each) is usually associated with the tunneling resistance r_i between them [78,107]. Indeed, as mentioned in Sec. III A, in those materials the statistically determined upper bounds that were found for the critical conductivity exponent, t, are also 2.6 in 2D and 4.0 in 3D [71,72], showing a striking similarity to the above porous media in which the conducting objects are slender [73].

As Archie's study and most works that followed it were concerned with sedimentary rocks [2,12,108], we turn now to show that in those systems the $\langle r_i \rangle \gg \langle r_f \rangle$ relation is to be expected. The simplest introductory model to such rocks is provided by the "random void" model [77]. This model consists of densely packed, nonpermeable, nonconducting spherical grains, between which there are pores that contain the electrically conducting liquid. The basic structure of this model, when one assumes equally sized spherical grains, is illustrated in Fig. 4. As seen in the figure, the void (or cavity) pores in the system are connected by very narrow throat (or neck) pores. Hence, if n_v is the concentration of the voids and V is the average volume of a void, the porosity of the whole system is closely approximated by $\phi \approx n_v V$. If the voids are considered as the sites in the system and the throats as the bonds (as in lattices [109] and in closely packed spheres [38]) the concentration of the throats n_t fulfills the relationship

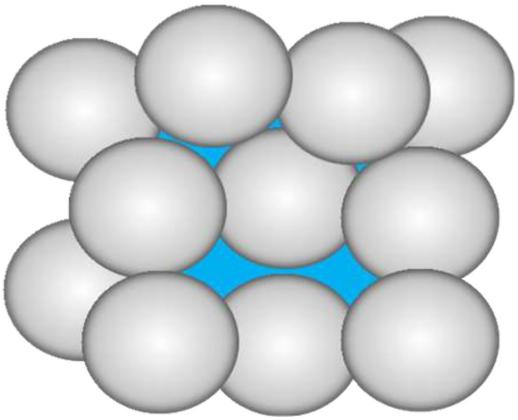

FIG. 4. An illustration of a volume element of the three-dimensional random void model. The spheres represent the nonpermeable nonconducting grains in the medium and the blue background represents the conducting liquid that fills the pores. One recognizes that there are two types of pores, the large volume voids and the small volume "throats," that connect neighboring voids. The important point to notice is that the total volume of the voids is much larger than the total volume of the throats, so that, practically, the macroscopic porosity of the system is much larger than the volume of the throats.

FIG. 5. An ensemble of stones that illustrates the basics of the dense solid-grain packing that is abundant in sedimentary rocks. As can be seen in the figure, the *total porosity is lower than that of the random void model* of Fig. 4, but as in that model, one can recognize that there are two groups of pores, those of the relatively wide aperture (the voids) and those of the narrow aperture (the throats). Note also that the pore spaces are connected [54,110], thus providing continuous conducting paths.

$n_t \approx n_v^2$. Using this basic relationship let us estimate the electrical resistance of the two types of pores. Starting with the voids, and assuming that the diameter of the spherical grains is w, the volume of the voids can be geometrically approximated by considering corresponding closely packed polyhedra [77] or by a sphere with an effective radius $a_v \propto w$. If the resistivity of the conducting liquid is ρ, the electrical resistance of such a liquid-saturated spherical void is $r_v = \rho/\pi a_v$. On the other hand, if the throat diameter is ε, its resistance r_t, when $\varepsilon \ll w$, can be approximated by $r_t = 4\sqrt{2}\rho w^{1/2}/\varepsilon^{3/2}$ [77]. Hence, in the present system of random voids connected by throats we have that $\langle r_t\rangle/\langle r_v\rangle \approx (\langle w\rangle/\langle\varepsilon\rangle)^{3/2}$, which means that $\langle r_t\rangle \gg \langle r_v\rangle$.

However, while the above random void model serves well as a simple introduction to sedimentary rocks, this model is associated with a relatively high porosity, which is on the order of 36%. Correspondingly, as such it does not provide a realistic model for sedimentary rocks of low porosity [12], i.e., when the total volume of the pores is considerably smaller than the total volume of the insulating grains in the system. Indeed, in general *the porosity in sedimentary rocks varies between 0.5% and above 36%* [110]. To examine the electrical conductivity in sedimentary rocks of low porosity, let us consider their structure as manifested by the abundant species of sandstones and limestones [54], in which the grains are not spherical in addition to having a distribution of sizes [36]. A useful illustration of such systems, as given here in Fig. 5, represents well ensembles of closely packed sedimentary rocks of variable size grains. As can be clearly noted, the porosity (the total volume of the pores between the stones) is very small in comparison with that of the above random void model of Fig. 4. Similarly, for porous media of very low porosities the high-porosity sedimentary rocks, even for very low porosities the pores belong to two distinguishable groups, those of relatively large volumes to which we also refer as voids, and the slimmer ones to which we also refer as throats. Indeed, a corresponding bimodal distribution of pores was observed in many sedimentary systems where the effective average size of the voids $\langle b_v\rangle$ is at least an order of magnitude larger than that of the average width of the throats $\langle\varepsilon\rangle$ [108]. Hence, as for the slender pore systems that were described above, the three relations $\phi \approx n_v V$, $n_t \approx n_v^2$, and $\langle r\rangle_t/\langle r_v\rangle \approx (\langle b_v\rangle/\langle\varepsilon\rangle)^{3/2} \gg 1$ are also expected in sedimentary rocks of low porosities. The first of these relations for very small ϕ values is that, while the voids remain interconnected [54], the $\phi_c \to 0$ relation that we discussed in Sec. II is maintained. The second relation follows the fact that, independent of the porosity, the pore system consists of series of void-throat connections [110], as was the case illustrated in Fig. 4 for the random void model with the relatively high porosity. The third relation reflects the fact that the pore size distribution in sedimentary rocks of low porosity is also found to be bimodal with $\langle b_v\rangle \gg \langle\varepsilon\rangle$ peaks [108,110].

Following the existence of the above three relations in many types of low-porosity media, we turn to their consequences for understanding the m value confinements in those media. For clarity, we do so by using the simplest and the most widely used representative model that exhibits these relations. i.e., the line segment (or the 2D stick) system that we introduced in Sec. II. Correspondingly the mapping of the above sedimentary rock model (with $\langle r_t\rangle \gg \langle r_v\rangle$, $n_t \approx n_v^2$, and $\phi_c \to 0$) on the line-segments model (with $\langle r_i\rangle \gg \langle r_f\rangle$ [86]) will enable now the explanation of the two features of Archie's law within the framework of percolation theory.

C. Analysis of percolation conductivity in the line-segment model

For simplicity, let us study the percolation behavior of systems of slender; permeable objects by considering the line-segment model that was introduced in Fig. 1. This follows our above conclusion that systems of slender pores can provide the $\langle r_i \rangle \gg \langle r_f \rangle$ relation. The simplicity associated with slender objects follows the fact that, while generally ϕ is not proportional to $n_{\rm f}$, in the case of slender pores represented by the line-segment model, these are practically proportional. This property can be appreciated by considering a system with a concentration $n_{\rm f}$ of randomly and isotopically distributed slender-permeable objects. In 2D for a system of rectangles of length L and width δ, such as in Fig. 1, the porosity of the system for the dominating isotropic orientation distribution of the rectangles (which yields a factor of $2/\pi$ [82]) is given by $\phi = n_{\rm f}(L\delta – B\delta^2/\pi)$. Similarly, in 3D, the porosity of the corresponding system is given by $\phi = n_{\rm f}(aL\delta^2 – bB\delta^3)$ for channels and $\phi = n_{\rm f}(aL^2\delta – bBL\delta^2)$ for fractures, where a and b are constants between π and 1, and B is the average number of intersections per given object. Since, for typical slender pores in porous media [3,4] $L/\delta > 10^2$, and since for typical $n_f > n_{fc}$ values, $L/\delta \gg B$ (the corresponding $B_{\rm c}$ values at the onset of percolation are only $B_c = 3.7$ in 2D and 2.8 in 3D [72,91]), one can neglect the second, small, term in ϕ. Consequently, in the following we simply use the linear approximation of $\phi \propto n_f$ [87,93]. Starting now with the simpler $r_f \gg r_i$ case we note that the electrical network of that model is, topologically, just the same as that of the classical lattice-percolation model [74–76] (see SM(2) in Ref. [56]) where the line segments (or the sections between adjacent intersections [87]) are considered to be the bonds in the system. Hence, by the latticelike percolation universality in the continuum [78], and as proven by our computer-controlled experiment for 2D line segments [87] and by recent simulations of others [92,99,100], we know that $\sigma \propto (n_f - n_{fc})^{\mu}$, where μ is the universal-critical exponent of the conductivity [74]. Following Eqs. (1) and (2) when $n_f \to n_{fc}$, we can replace the values of m or t [93] (see SM(1) and SM(2) in Ref. [56]) by the universal μ, finding then that

$$\sigma \propto (1/r_{\rm f})(n_{\rm f} - n_{\rm fc})^{\mu} \propto (1/r_f)(\phi - \phi_{\rm c})^{\mu}. \tag{3}$$

Turning from that rather standard case to the other extreme $r_i \gg r_f$ case, one would expect (on the basis of the universality of percolation as a phase transition [74,76,78]) that the system's global conductivity will be determined by the higher-value resistors that are necessary for the onset of percolation (see SM(3) in Ref. [56]). Hence, in that $r_i \gg r_f$ case we expect, following the universality that extends also to the lattice-site percolation [74,109], that $\sigma \propto (1/r_i)(n_i - n_{ic})^{\mu}$, where $n_{\rm i}$ is the concentration of the resistors associated with the intersections and $n_{\rm ic}$ is the corresponding threshold for the conductivity in their network. Indeed, this dependence is confirmed in simulations by us [86] and by others [92], on line-segment 2D systems as well as on line-segments like 3D systems [91]. However, while *a priori* the value of $n_{\rm i}$ (unlike the value of $n_{\rm f}$) in such systems is not known (or controllable), it is clearly proportional to the probability $P_{\rm i}$ that a slender object, such as a line segment, will be intersected by another one. Since $P_i \propto n_f$ (as expressed, e.g., by $B = V_{ex}n_f$) and since the number of slender objects in the system is $n_{\rm f}$, the total number of intersections in the system is given by $P_i n_f \propto n_f^2$. This is easy to appreciate intuitively by noting [38,100,109] that the doubling of $n_{\rm f}s$ will quadruple the $n_{\rm i}s$, so that $n_i \propto n_f^2$. Indeed, this simple $n_i \propto n_f^2$ expectation has been confirmed by simulations [92] of the 2D system of line-segment–like "sticks." The generalization of the above results to a 3D system of intersecting fractures is straightforward, noting that (as in Fig. 2) each intersection requires the presence of two fractures, so that again $n_i \propto n_f^2$. Since, as mentioned above, the intersection volume is negligible compared with the volume of the individual slender objects, we have that $n_i \propto n_f^2 \propto \phi^2$, and this yields that

$$\sigma \propto (1/r_{\rm i})(n_{\rm i} - n_{\rm ic})^{\mu} \propto (1/r_{\rm i})\left(n_{\rm f}^2 - n_{\rm fc}^2\right)^{\mu} \propto (1/r_{\rm i})\left(\phi^2 - \phi_{\rm c}^2\right)^{\mu}. \tag{4}$$

Comparing this result for $r_i \gg r_f$ with the result of Eq. (3) for $r_f \gg r_i$, we note that in the limit of $n_f \to n_{fc}$ (i.e., for $\phi \to \phi_c$) one gets [86,92,99,100], as expected from the phase transition-like universality of percolation [74,76], the same $\sigma \propto (\phi - \phi_c)^{\mu}$ dependence. This is regardless of the $r_{\rm i}/r_{\rm f}$ ratio. On the other hand, in the $r_i \gg r_f$ scenario of Eq. (4) we also get that for $n_f \gg n_{fc}$

$$\sigma \propto (1/r_{\rm i}){n_{\rm f}}^{2\mu} \propto (1/r_{\rm i})\phi^{2\mu}. \tag{5}$$

The important finding here is that unlike the $r_f \gg r_i$ scenario of Eq. (3), we have that for the latter $r_i \gg r_f$ scenario the further increase of ϕ above ϕ_c in Eq. (4) yields an increase of the conductivity exponent from μ to 2μ. This indicates a behavior that we associate later with a more general phenomenon that we call an electrically affected connectivity. Now we recall, as noticed in the Introduction and in Sec. III A, that groups of m values derived from data analysis by applying Archie's law as given by Eq. (1), were found to be limited by 2.6 or by 4.0 [38,40] in many porous media. The fact that these values are the same as those of the universal percolation 2μ(2D) and 2μ(3D) exponents that we predict in Eq. (5), suggested to us that the m results that are determined from the observations by their analysis according to Archie's law, are simply due to the m values confinement to the μ–2μ interval. The fact that the universal-critical exponents determine the bounds of this interval further suggested to us that they represent an extension of the critical behavior of the percolation phase transition to higher ϕ values in the corresponding porous media. This is in spite of the large $\phi/\phi_c \gg 1$ relation.

However, such a conclusion as manifested by Eq. (5), is *a priori* counterintuitive and hard to grasp within the common framework of the theory of percolation as a phase transition [74,76]. This is because in second-order phase transitions in general, and in the percolation transition in particular, the critical behavior (manifested here by the universal exponent μ) is associated with the $n_f \to n_{fc}$ limit, while for Eq. (5) to be effective one must have that $n_f \gg n_{fc}$ (or $\phi \gg \phi_c$). To consider these seemingly contradictory requirements, let us dwell a bit on the ϕ (or $n_{\rm f}$) range in which Eq. (5), that involves the universal-critical μ value, is expected to be valid.

D. The percolation to effective medium transition in porous media

Generally, as ϕ (i.e., n_f) increases between ϕ_c and $\phi = 1$, there are two distinguishable asymptotic regimes: the dilute, percolation critical regime that we have discussed thus far (Eqs. (3)–(5) and SM(2) in Ref. [56]) and a denser regime that is known as the effective-medium (EM) regime. Since Refs. [38] and [96] provide excellent reviews of the latter regime, we describe it here only in the simplest terms that are necessary for the present work. We do so by comparing the effect induced on the $\sigma(\phi)$ dependence, by the adding of a bond resistor to the system in each of these regimes. The dominant effect of such an addition in the above-threshold dilute-percolation regime is to increase the geometrical, and thus the electrical, connectivity of the system by creating an additional connecting path (see SM(2) in Ref. [56]). In contrast, in the denser EM regime the connected network is already well established, and the dominant effect of the added bond resistor is to connect in parallel to an existing bond, i.e., to increase the average local conductance and thus to increase the global conductivity of the network [109]. The effects of the above additions can be appreciated visually by adding a line segment to the systems that are illustrated in Fig. 1. There, an added line segment can either connect two segments that have not been connected before, or add a connection between two segments that are already connected. The first type of connection is the dominant one in the dilute percolation regime, while the second type of connection is the dominant one in the denser EM regime.

To consider the above two regimes in porous media, let us return to Fig. 5. In sedimentary rocks of low-ϕ systems, the main effect of the increase of ϕ is to increase the concentration of throats, which in turn increases the number of possible current paths (i.e., the connectivity) in the system. In contrast, in the denser EM regime, the main effect of the increase of ϕ can be to enlarge the volume of the individual voids [108,110] and/or to cause their clustering [111]. (In composite materials, the latter effect is known as the bundling of the conducting elements [97] in the already geometrically connected system.) Now we note that having a system that is still conducting at a very low ϕ means also that its $\phi_c \to 0$. On the other hand, if ϕ_c is large, there will be a relatively small ϕ range (between ϕ_c and 1) in which the EM conditions determine the conductivity, and thus the extrapolated threshold of the corresponding EM regime, ϕ_{ec}, will be somewhere within this range, as determined in many experimental and computational works [96,109] (see Appendix A). Since the values of ϕ_c and ϕ_{ec} result from very different reasons one does not expect a dependence of ϕ_{ec} on ϕ_c (except of course that $\phi_{ec} > \phi_c$). Indeed, it has been concluded previously that there is no correlation between these two parameters in porous media [79]. As will be discussed below, for the present work the important point is that in conducting porous media of low porosity, such as that of sandstones, the typical corresponding ϕ_{ec}/ϕ_c value is on the order of 30–40 [79]. Obviously then, the outcome of the different effects of the bond-resistor additions in the above two regimes will cause different $\sigma(\phi)$ dependencies in those regimes. Correspondingly, while the asymptotic $\sigma(\phi)$ dependence of Eq. (3) accounts for the dilute-percolation regime, the $\sigma(\phi)$ behavior in the asymptotic EM regime is given by [38,96]

$$\sigma(\phi) \propto (\phi - \phi_{ec})^{u}, \tag{6}$$

where ϕ_{ec} (or x_{ec}) is the corresponding calculated [38], simulated [109], or experimentally derived [96,111], by extrapolation of the conductivity data in that regime, and $u \equiv 1$ is the universal EM exponent for all dimensions. In passing, we remark here that both $m < 1$ [39,79] or $t < 1$ [93] values (see SM(3) in Ref. [56]) were previously shown to be associated with correlation effects in the structure and thus, these rather rare effects are not considered in the present work.

As is to be expected from the above discussion, and as was well demonstrated in Ref. [109] and many other works, there is a smooth transition from the dilute-percolation regime of Eq. (3) to the dense-EM regime of Eq. (6). Following that, we further conclude that with the increase of ϕ, the transition between the two regimes will be manifested by a continuous decrease of m from $m = \mu$ to $m = u \equiv 1$. It is also obvious (see Appendix A) that the smaller the ϕ_c, the larger the ϕ regime in which the $\phi_c \ll \phi < \phi_{ec} < 1$ condition can be fulfilled. Correspondingly, the larger will be the ϕ regime where the critical μ exponent (rather than the EM, u exponent) will be observed. An experimental justification for this argument is provided by the findings that in some porous media, $1 \leqslant m \leqslant \mu$ values have been observed [43], while for others, where the pores were slender (i.e., where $\phi_c \to 0$, see Sec. II), only $m = \mu$ values have been found in the studied ϕ range. In particular, such $m = \mu$ values have been found for ϕ/ϕ_c ratios, as large as $\phi/\phi_c = 20$ [2,19,54,79]. Similarly, for composite materials with slender conducting particles and $x_c \to 0$, the universal $t = \mu$ value has been observed up to x/x_c values that are as high as 100 [97]. These observations are in sharp contrast with those of systems of, say, spherical [112] or spherical-like [113,114] objects where $x_c > 0.16$, and thus (since $x \leqslant 1$) the value of x/x_c cannot be larger than 6. In other words, for slender objects for which ϕ_{ec} (or x_{ec}) are much larger than ϕ_c (or x_c) there will be a wide enough ϕ/ϕ_c (or an x/x_c) interval where the critical behavior of Eq. (3) will be observed, before (i.e., for $x < x_{ec}$) the domination of the EM effect. Simulations that were reported for the above-considered line-segment systems [92] fulfill that expectation. In those simulations, a $t = \mu$ to a $t = 1$ transition was found to take place with the increase of n_f, over a large n_f/n_{fc} regime. Following the above, we suggest that the aforementioned experimental and simulation results provide convincing evidence that for slender objects, a wide observable critical-percolation regime can be obtained before the EM effect dominates the $\sigma(\phi)$ [or the $\sigma(x)$] dependence. *The general "practical" point to be noticed here is that except for the onset of the EM conditions, there is, in principle, no limit to the width of the critical regime in which m values that are confined by the percolation universal exponents of the electrical conductivity can be observed.* For the line-segment system studied here, this implies that there is a wide $\phi \gg \phi_c$ (or $x \gg x_c$) range in which the system is still dilute and thus its electrical properties, as reflected by the exponent μ, are controlled by the percolation Nodes Links Blobs (NLB) connectivity (see SM(2) in Ref. [56]) connectivity. As discussed in Appendix A, the latter suggestion and conclusion are well supported by the fact that the proximity to the percolation

threshold is more amenably represented by the $(\phi - \phi_c)/\phi_c$ [or the $(x - x_c)/x_c$] parameter [72,100], than by the more commonly used $(\phi - \phi_c)$ [or the $(x - x_c)$] parameter [74].

E. The solution to Archie's *m*-values puzzle

In Sec. II we have shown that ϕ_c (or x_c) decreases with the increase of the slenderness (i.e., the aspect ratio) of permeable [3] and nonpermeable [73] objects. Considering the fact that in porous media there are numerous systems in which $r_i \gg r_f$ or $r_t \gg r_v$ (see Sec III B), we have shown in Sec. III C on the basis of Eqs. (3)–(5) that in the percolation critical regime a high r_i/r_f, or a high r_t/r_v ratio can yield conductivity exponents between μ and 2μ. In Sec. III D and Appendix A we have shown that a system that still conducts at very low porosity can have a relatively wide $(\phi - \phi_c)/\phi_c$ range in which the critical behavior may be observed. Moreover, for systems with a high r_i/r_f or a high r_t/r_v ratio, an increase of m with ϕ, from $m = \mu$ to $m = 2\mu$ (or part of it, due to the onset of the EM conditions) is expected to take place [see Eqs. (3)–(6)]. Consequently, since both the $\phi_c \to 0$ condition (see Sec. II) and the very high r_i/r_f or r_t/r_v conditions do exist in numerous porous media (see Sec. III B) the confinement of the m values between $m = \mu$ and $m = 2\mu$ is expected to be a dominant characteristic of those media. This conclusion is confirmed by the observations (see Sec. I and SM(1) in Ref. [56]) on both porous media and composite materials, for which the experimentally derived m [38] or t [71] values were found to be between 1.3 and 2.6 [i.e., between μ(2D) and 2μ(2D)], or between 2.0 and 4.0 [i.e., between μ(3D) and 2μ(3D)]. *This exact agreement between our expectations, which are based on well-founded percolation theory [*[74], [78]*], and the experimental statistical conclusions regarding the confinements of the m and t values [*[38], [71]*], provides then a solution to the m-exponent puzzle of Archie's law.* In passing, we remark that in the case of composite materials these confinements take place when the conducting particles are slender [73] and the $r_i \gg r_f$ condition is provided by the much higher tunneling resistance of the intersection junctions between the particles, in comparison with that of their own resistance [107].

To summarize the above predictions, in Fig. 6 we present an illustration of them by our expected dependence of the exponent m on $\log_{10}[(\phi - \phi_c)/\phi_c]$ in three-dimensional porous media. Accompanying this, we show that our predictions are confirmed by numerous results on porous media, in which the analysis of the data was carried out according to Archie's law, as given by Eq. (1). In particular, Fig. 6 presents our main prediction for the designated area between the solid-red curve and the dashed-blue curves, into which all the numerous experimental m values that were derived by applying Archie's law in porous media can be fitted. Below, we call that area the "m-ϕ phase space."

The first and most significant prediction of our theory [see Eqs. (3)–(6)] is that Archie's m values for 3D porous systems will be between $\mu(3D) = 2$ and $2\mu(3D) = 4$, and/or between m values in that interval and $m = u = 1$. This is in contrast with other theories that predicted specific [54] or non-confined [115] larger than μ values for the conductivity critical exponent in the continuum (see SM (3) in Ref. [56]). The curves shown in Fig. 6 represent the predicted dependencies of said

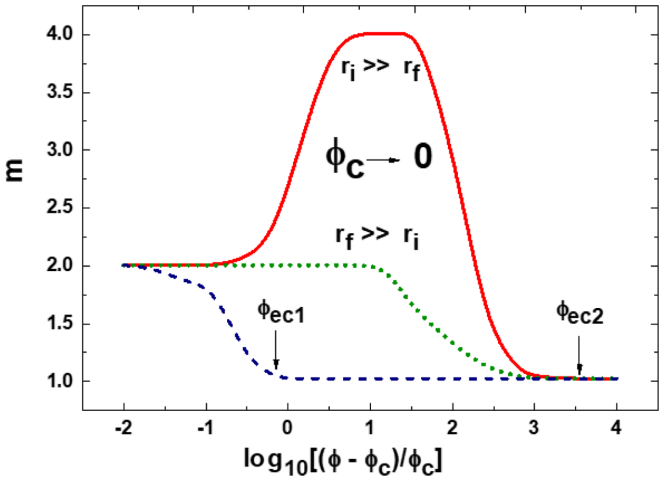

FIG. 6. An illustration summarizing the results obtained in this work for the dependence of Archie's conductivity exponent m on the normalized proximity to the percolation threshold $\log_{10}[(\phi - \phi_c)/\phi_c]$. This particular scale for the proximity parameter encompasses the range of the great majority of the many $m(\phi)$ data available in the literature. The dashed-blue curve represents the common percolation to effective medium transition, i.e., from $m = \mu = 2$ to $m = u \equiv 1$. The dotted-green curve and the solid-red curve represent the $m(\phi)$ dependencies when the threshold porosity $\phi_c \to 0$. The solid-red curve is for the $r_i \gg r_f$ case and the dotted-green curve is for the $r_f \gg r_i$ case. The ϕ_{ec1} value indicates the onset of the effective medium conditions when $(\phi_{ec1} - \phi_c)/\phi_c \leqslant 1$, while the ϕ_{ec2} value indicates this onset when $(\phi_{ec2} - \phi_c)/\phi_c \gg 1$. As shown below, the predictions presented in the figure are confirmed by the numerous experimental results that were found on both fractured rocks and sedimentary rocks.

m values on $\log_{10}[(\phi - \phi_c)/\phi_c]$. These are the dotted-green curve, the solid-red curve, and the dashed-blue curve, respectively. The fact that numerous statistical and particular m values that were reported in the literature [2,4,6,19,38–43] "fall" within our m-ϕ phase space provides solid confirmation for the most important prediction of our work above, i.e., the confinement of the m values to our m-ϕ phase space.

The span of the $\log_{10}[(\phi - \phi_c)/\phi_c]$ range over which we predict the m values to be observed is also confirmed by the results in the literature [2,19,39,79]. Here we note that, while many determinations of m from the $\sigma(\phi)$ data were carried out taking $\phi_c = 0$, we (see Sec. II) as others [2,6,54,79] have shown that ϕ_c has always a finite value, and that the data fits with $\phi_c = 0$ simply reflect the limited accuracy of the determination of very small porosities in porous media [47,81]. On the other hand, we note that the finite ϕ_c values have been determined theoretically [3,76,77,82,91] to be between 0.29 and 0.03, and empirically to be between 0.36 and 0.05 [6,79,110]. Correspondingly, considering the ϕ ranges used in the various studies (see, e.g., Refs. [6,19,39,79]) we have established that the $\log_{10}[(\phi - \phi_c)/\phi_c]$ range that we present in Fig. 6 encompasses the numerous available experimental results [2,6,38,39] from which Archie's m values were extracted. In particular, the extreme ends of the $\log_{10}[(\phi - \phi_c)/\phi_c]$ scale shown in Fig. 6 were as follows. The small $(\phi - \phi_c)/\phi_c$ extreme is at $(\phi - \phi_c)/\phi_c = 0.1$ [91] and the large $(\phi - \phi_c)/\phi_c$

extreme is at $(\phi - \phi_c)/\phi_c \approx 100$ [19,79]. We have to add here that, in principle, these scales can be extended by improving the accuracy of the experimental results, and/or the data analysis for the small $(\phi - \phi_c)/\phi_c$ values, and by the ability to determine very small ϕ_c values for the large $(\phi - \phi_c)/\phi_c$ values. Moreover, the relative position of ϕ_{ec2} at the end of the latter $(\phi - \phi_c)/\phi_c$ range in the figure is also consistent with previous evaluations of data that were analyzed by Archie's law [79]. Hence, our basic prediction of the confinements of the m values to the designated m-ϕ phase space that is shown in Fig. 6, is confirmed by the numerous experimental results that were obtained by the application of Archie's law for the analysis of the data. The other important confirmations of our predictions concern the $m(\phi)$ dependencies within the m-values confinement and the $\log_{10}[(\phi - \phi_c)/\phi_c]$ range that are shown in Fig. 6. Indeed, there are many experimental observations for the increase [7,40,53,116,117], the decrease [19,53,106,118], or a peak in the $m(\phi)$ dependence [44] over intervals within the $\log_{10}[(\phi - \phi_c)/\phi_c]$ range in the figure.

Turning to the physics involved in Fig. 6 we recall that the lower dashed-blue curve in the figure represents the classical-lattice $m(\phi)$ transition from the percolation regime (see SM(2) in Ref. [56]) to the EM regime [109] (see Sec. III D). Considering this curve, we remark that in ensembles of spherical pores [2,91] or in granular metals of nearly spherical particles [113,114], where the percolation threshold is not small, the onset of the EM conditions at ϕ_{ec1} that must be between $\phi = \phi_c$ and $\phi = 1$ is not far from ϕ_c, and thus $(\phi_{ec1} - \phi_c)/\phi_c < 0.3$ (see Appendix A). The upper two curves in Fig. 6 represent the $m(\phi)$ dependencies in the cases of slender pores or small-volume voids, throughout the $0 \leftarrow \phi_c \ll \phi < \phi_{ec2}$ range. The higher (solid-red) curve illustrates the possible $m(\phi)$ [or $t(x)$] depenence when $r_i \gg r_f$, or $r_t \gg r_v$, and the lower (dotted-green) curve represents this behavior when these two inequalities are reversed. In general, for the less extreme r_i/r_f or r_t/r_v ratios, the salient qualitative features of the upper solid-red curve will be maintained, but the highest m value observed may be smaller than $2\mu(3D)$ ($m = 4.0$ here). This is due to the onset of the EM conditions at a smaller ϕ value than the one required for reaching the $2\mu(3D)$ peak [see Eq. (4)]. Our prediction as manifested by that curve accounts for all the intermediate $\mu < m < 2\mu$ values that were found in related simulations [22,92] and in many experimental studies [2,38] (see Sec. I and SM(1) in Ref. [56]). *The very general prediction that we make here is that for all cases, the m (or t) values will always be confined to the area between the upper* (*solid-red*) *curve and the lower* (*dashed-blue*) *curve*. The overall feature exhibited in Fig. 6 is the rise of m towards its maximum value that is $\leqslant 2\mu(3D) = 4.0$, and the subsequent decrease of m towards $m = 1$. *The other implied feature is that* according to the percolation or the EM regime that applies to the corresponding ϕ, *the plateau in the m values can be obtained only for the* $m = 2.0$, $m = 4.0$, *or* $m = 1$ *values*. These features are based on our predictions that the $m(\phi)$ dependence is determined by two global parameters, the ϕ_{ec}/ϕ_c ratio and the r_i/r_f, or the r_t/r_v, ratio. In other words, according to our analysis, the existence of both a large ϕ_{ec}/ϕ_c value and a large r_i/r_f value, or a large r_t/r_v value, ensures the observation of $\mu < m < 2\mu$ values over a large $(\phi_{ec} - \phi_c)/\phi_c$ range.

Establishing that the agreement between the experimental results and the features exhibited in Fig. 6 is indeed due to the mechanisms that we suggested above, let us recall now that the high values of the above ϕ_{ec}/ϕ_c and r_i/r_f (or the r_t/r_v) parameters are simultaneously fulfilled by the porous media of concern in the present work. In particular, we note that the original results of Archie [1] and the many observations that followed [38] were on various sedimentary rocks for which high ϕ_{ec}/ϕ_c [79] and high r_t/r_v, (via the high $(\langle b_v\rangle/\langle\varepsilon\rangle)^{3/2}$ [110]) ratios have been determined (see Sec. III B). Moreover, the increase of m with the increase of $\langle b_v\rangle/\langle\varepsilon\rangle$, and with the increase of ϕ in simulations of tight sandstones [22], leaves no doubt concerning the applicability of our percolation model to porous media for which features such as illustrated in Fig. 6 are observed. In fact, we can further expect from the richness of pore sizes and their configurations in porous media that there will be numerous systems where the above two ratios are simultaneously large, and that this is the reason for the wealth of m confinement data that are summarized in Refs. [2,38,39,44]. For completeness, let us mention now porous media where only one of the above ratios is high. Considering a high ϕ_{ec}/ϕ_c as in low-porosity sedimentary rocks [79] but in which the pore distribution is quite homogeneous [54] (say, $\langle b_v\rangle \approx \langle\varepsilon\rangle$ and thus $r_t \approx r_v$), we predicted the critical behavior with only $m = \mu$ values over a large $(\phi - \phi_c)/\phi_c$ range [see Eq. (3)]. Indeed, such behavior has been observed in many sedimentary rocks [1,19,54]. The other extreme is the case of a relatively small $(\phi - \phi_c)/\phi_c$ ratio (due to as large as $\phi_c = 36\%$) but a large r_t/r_v ratio [due to a large $(\langle w\rangle/\langle\varepsilon\rangle)^{3/2}$], as in the random void model (see Sec. III B). In that case a transition from the $m = \mu$ to the $m = u \equiv 1$ value may be observed [43], while higher, $m > \mu$, values are likely to be observed due to other effects [53,77] (see also SM(3) in Ref. [56]) than the one suggested in the present work. Regarding the latter extreme case we point out, however, that none of the previously proposed mechanisms for the interpretation of the m values can account for the statistically proven sharp decrease in the experimental observations at $m = 4.0$ [38], as does our presently suggested mechanism with the $m \leqslant 2\mu$ limitation.

An important prediction made in Fig. 6 is the dependence of m on r_i/r_f, that can be appreciated by considering the possible "vertical" increase (i.e., for the same ϕ) of m within the $\mu \leqslant m \leqslant 2\mu$ confinement range. The validity of this prediction is strongly supported by the simulation results of the line-segment model of Ref. [92], when adopted to porous media of slender pores, and by the simulation results of Ref. [22] for sedimentary rocks in which the $m(\phi)$ and the $m(\langle b_v\rangle/\langle\varepsilon\rangle)$ dependencies have been determined. The importance of having these $m(\phi)$ and $m(r_i/r_f)$ dependencies is their universality as well as their usefulness. As a demonstration of the latter let us recall the simple model that we have suggested in Sec. III B for sedimentary rocks of low porosity, and for which we concluded that $\langle r_t\rangle/\langle r_v\rangle \approx \langle b_v\rangle/\langle\varepsilon\rangle^{3/2}$. For such rocks a large m value, within the possible $\mu < m < 2\mu$ confinement interval, would indicate a relatively large $\langle b_v\rangle/\langle\varepsilon\rangle$ ratio. In other words, the variation of m with ϕ can provide information on how the microstructure of the porous medium changes with the variation of ϕ. In practice, one can apply the relatively easy to perform 3D simulations of electrical

conductivity as a function of n_f (i.e., of ϕ) for reasonable $\langle r_i\rangle/\langle r_f\rangle$ or $\langle r_t\rangle/\langle r_v\rangle$ values, and then derive the W/ε or the $\langle b_v\rangle/\langle\varepsilon\rangle$ variations with ϕ by comparison to the experimentally found $m(\phi)$ dependence. This may further enable the derivation of information on variations of the distribution functions of these structural parameters. The above analysis responds then to the old well-known request of Ref. [54] to correlate the value of m with the pore structure in the porous medium, but unlike in previous attempts, here this is done within the framework of the well-established phase transition of percolation theory.

Another complementary effect that we found during this work is that for exactly the same geometrical-topological network of *slender pores*, a high $\langle r_i\rangle/\langle r_f\rangle$ ratio will not only induce the confined $\mu < m < 2\mu$ values but will also expand the effective percolation critical regime of conductivity that is geometrically determined by the ϕ_{ec}/ϕ_c ratio. This effect and its importance are considered in Appendix B. However, for clarity, in Fig. 6 we used the same ϕ_{ec2} for both extremes of the r_i/r_f ratios.

Finally, we must stress here, of course, that the m values within, or outside, the confined regime, can also be obtained due to other effects (see e.g., SM(3) in Ref. [56]). However, unlike the predictions of the present work, we do not know of any other explanation that can account for the sharp statistical drop of the experimentally observed [38,71] m values at $m = 2.6$, or $m = 4.0$. This leaves us with the conclusion that the majority of the m values that were observed within the above m-confined intervals are due to the reasons that we proposed in the present work.

F. Geometrically and electrically affected connectivities

In the course of this work, we noted a percolation-related property that we call an electrically affected connectivity. To introduce the physical basis of this property, we start by reexamining Eqs. (3) and (4). Comparing these two equations, one notes that, while the system's information in Eq. (3) is given by the two parameters that characterize the initially introduced conducting objects, n_f and r_f, the information in Eq. (4) is given by n_f, and r_i, where the latter is an entity that is, *a priori*, not related to the system of $n_f s$. The question that arises then is whether the topology of the resulting dominant electrical network will change when the r_i/r_f ratio is varied. To answer that question consider an electrical network of r_1 and r_2 resistors. Commonly, such a network is presented by an NLB network (see SM(2) in Ref. [56]) except that all the r_1 and r_2 resistors are replaced by some effective-average resistance r [96,109,115]. Now let us consider two cases. First, we assume a system in which there is a mixture of n_1 of the r_1s and n_2 of the r_2s such that the concentration of each kind of resistor is enough to induce percolation (i.e., n_1 is larger than its critical concentration n_{1c}, and $n_2 > n_{2c}$). Correspondingly, each of the two independent electrical networks is above its threshold, and thus a corresponding NLB model can describe its network. In that case, for a given geometrical network of n_1s and n_2s, the increase of the r_2/r_1 ratio will be manifested not only by a change of the prefactor of the global conductivity σ [see Eqs. (3) and (4)], but also by a change from the $\sigma \propto (1/r_2)(n_2 - n_{2c})^{\mu}$ dependence to the $\sigma \propto (1/r_1)(n_1 - n_{1c})^{\mu}$ dependence. In other words, while the increase of r_2/r_1 did not change any details of the geometrical topology of the entire system, it did change the dominating network that determines the overall conductivity, favoring the network of lower-value resistors. Let us turn now to the second alternative, where n_1 and n_2 are such that both, some r_1 and some r_2, resistors are necessary for the onset of percolation. In this case, in contrast to the former case, the increase of r_2/r_1 will yield a network in which the higher-value resistors will dominate the global conductivity of the system. Such is the scenario we described in Fig. 1, where both the r_f resistors of the line segments [87] and the r_i resistors of their intersections [86] are inherently necessary for the formation of a conducting network. As concluded in Sec. III C in that scenario, the increase of the r_i/r_f ratio drives the system from the behavior of Eq. (3) to the behavior of Eq. (4). This shows that the change of the power-law parts of the corresponding dependencies represents the transition from the r_f-dominated topology to the r_i-dominated topology. In other words, the corresponding electrically induced change in the connectivity is reflected by the change in the value of m, which is the critical exponent of the global electrical conductivity of the system. We see then that the change of m with the "vertical" (i.e., for the same ϕ) increase of r_i/r_f in Fig. 6 is due to a variation of the connectivity of the electrical network. This reveals that the $\mu \leqslant m \leqslant 2\mu$ confined values represent a phenomenon of an "electrically affected connectivity." As we see here, this concept is useful for describing scenarios like those in the systems that are examined in the present work, where the necessary information of the system that is available is mixed. In such systems we know *a priori* only n_f (or ϕ) and the domination of r_i, rather than the r_f-n_f pair, or the r_i-n_i pair. To find then the $\sigma(n_f)$ dependence of the global conductivity one must have a "bridging relation" between the two ns, which may not be known. In the systems considered in this article (see Secs. III B and III C), this "bridge" is the $n_i \propto n_f^2$ relation that enables the derivation of Eq. (4). In particular, obtaining that relation leads us to understanding the m values and their $\mu \leqslant m \leqslant 2\mu$ confinements in porous media where the connections between the pores are much more resistive than their own resistance (see Sec. III B). Hence, the observed m-values confinement and their variation with ϕ, when the experimental data are analyzed according to Archie's law, is a manifestation of the transition in the corresponding electrically affected connectivity.

IV. DISCUSSION

Before discussing our solution to the puzzling success of Archie's law in describing the $\sigma(\phi)$ dependence in porous media, let us turn to an evaluation of the current state of understanding of this law prior to the present work. Considering such an evaluation, it was apparent to us that in view of the numerous attempts that have been made to account for its success, it would be impossible, within the scope of the present paper, to discuss those attempts beyond the short review that was given in Sec. I. On the other hand, we found that the outcome of these attempts in the 78 years that followed Archie's findings can be summarized by some typical quotes from the more recent literature, as follows. In 2000, it was concluded

that Archie's law is "strictly a parametrization used for curve fitting with *a priori* no physical meaning" [8]. Later, in 2009, it was proposed to give up trying to understand Archie's law by stating that "porous media is too complex and variable to be actually described by single models: e.g., empirical equation a la Archie" [45]. In 2013, it was concluded that "Despite the popularity of Archie's law, parametrizing bulk electrical conductivity as a power-law function of porosity seems to lack support from first principles" [7]. Our suggestion in Sec. I that Archie's law is a puzzle that calls for a solution is echoed in the 2015 evaluation that "Despite extensive use of Archie's law and significant research, the question of the numerical value of m and its dependence on the rock morphology has remained unresolved" [40]. Such evaluations have not changed in more recent years. In 2017 it was suggested that "a clear understanding of Archie's equation is lacking" [39] and the law was characterized as "inadequately understood" [48]. In 2018 it was concluded that "the physical basis of Archie's law has not been fully understood yet" and that "At present there is no consensus on the physical meaning of m in geological materials and further studies are still necessary to reconcile the existing findings" [11]. Hence, as such evaluations of Archie's law continue even today, the understanding of it has been limited to the conclusion that the m values are due to an unspecified "variety of factors" [38]. From the above short review, one must conclude that until now, Archie's law remained an unsolved puzzle.

In a contrast to the many past and present trials to account for Archie's law [39], as reflected by the above quotes, our present work provides not only a well-based physical understanding of the two features of Archie's law, i.e., the $\phi_c \to 0$ and the confinements of the m values, but also the relation between them. To substantiate this claim, let us return to the introduction of this paper, where we briefly reviewed the main common observations that were found for Archie's m exponent in porous media, and the corresponding t exponent in composite materials. This is done in order to show that all those observations are well accounted for by our analysis that rests only on the simple and firm foundations of the theory of continuum percolation [78] as a phase transition. In the introduction and in SM(1) of Ref. [56], we actually noticed that there are six typical behaviors that were experimentally observed for the values of m. Let us consider them now in light of our present predictions that are summarized in Fig. 6. First, the observed m values between 1 and 1.3 [43] and between 1 and 2.0 [6] confirm our conclusion concerning the existence of a transition from the percolation conductivity exponents $\mu(2D)$ and $\mu(3D)$ to the effective medium exponent ($u = 1$) in porous media. That this transition is expected to be observed in systems such as the ones considered in the present work is exhibited by the simulation results, such as those of the 2D line-segment systems that were reported in Ref. [92]. Second, the finding of the m-value confinement in the interval of $\mu(2D) = 1.3 \leqslant m \leqslant 2.6 = 2\mu(2D)$, in the same reservoir [40–42,54], is in accord with our Eqs. (4) and (5). In particular, this finding is applicable to porous media in which an aerial view of a fracture farm [80,90] shows the same features as the line-segment ensembles of Fig. 1. Third, the general confinement of m values between $\mu(3D) = 2.0 \leqslant m \leqslant 4.0 = 2\mu(3D)$ values in numerous porous media [4,38,39] confirms the predictions that we presented in Fig. 6 for 3D systems with a bimodal but correlated distribution of the conducting pore elements. Fourth, our prediction of the increase of m with the increase of ϕ within the confined $\mu < m \leqslant 2\mu$ intervals [see Eq. (4)] has been found in many porous systems [7,40,44,53,116,117]. Fifth, the widely observed decrease of $m(\phi)$, from a high value in the $\mu < m \leqslant 2\mu$ interval towards the $m = u \equiv 1$ value [19,44,53,106,118], further confirms our prediction for the final transition from the extended percolation regime to the effective medium regime at relatively high values of ϕ. In fact, a confirmation of our prediction of the increase, that is followed by a decrease of m with the increase of ϕ, as illustrated in Fig. 6, was found in controlled experiments in which m increased (from 1.3 to 1.5) and then decreased (from 1.65 to 1.40) with the increase of ϕ [44]. Moreover, very convincing support for this conclusion is provided by the simulation results of the increase of m with ϕ in void-throat systems [22] and for 2D system of permeable sticks [92] (as in Fig. 1). Here we note that in the latter simulations, unlike available experiments, the study of a wide range of n_f (or ϕ) values is possible, which enables us to establish firmly that the increase of m, from μ to an $m > \mu$ value with the increase of n_f, is followed by its decrease with the further increase of n_f. Sixth, we have shown that our prediction for an Eq. (3)→Eq. (5)→Eq. (6) transition is fulfilled by the observations on systems of slender conducting pores (such as cracks, fractures, and channels [3–6,67,68,71,74]) or low-porosity sedimentary rocks [108,110], i.e., for systems in which Archie's $\phi_c \to 0$ feature applies (see Sec. II).

Let us turn now to the steps that enabled us to establish the above agreements between our predictions and the aforementioned experimental and computational data. In Sec. III B we have shown that the slenderness of the pores can provide large r_i/r_f ratios in porous media, and in Sec. III C we have shown, by Eq. (4), that this large ratio is the necessary condition for the confinement of the m values in the $\mu \leqslant m \leqslant 2\mu$ interval. On the other hand, as shown in Sec. II, the slenderness of the pores yields the $\phi_c \to 0$ feature which we have shown in Sec. III E to be the necessary condition for observing the critical behavior before the (higher ϕ values) onset of the effective medium conditions. Similarly, in Sec. III B we have shown that the basic geometrical and electrical consequences that apply to slender pores apply also to the original [1], and very widely studied, sedimentary rocks of low porosity [2,12,110]. In particular, in those rocks the high ratio of the void-pore size to the throat-pore size (i.e., $\langle b_v \rangle / \langle \varepsilon \rangle \gg 1$) ensures the $r_i \gg r_f$ relation. This bimodal distribution of two types of resistors and their sequential connections [i.e., the $n_i \propto n_f^2$ relation; see Eq. (4)] ensures not only the $\mu < m \leqslant 2\mu$ confinement feature of Archie's law but also the increase of m with ϕ in those rock systems [22]. On the other hand, the $\phi_c \to 0$ feature in sedimentary rocks that conduct at very low porosities enables the observation of m values in that confinement range.

Considering the above comprehensive agreement between our predictions and the experimental manifestations of Archie's law [2,38] we recall that none of the previous models [39] could account simultaneously for the six behaviors that were mentioned above. In particular, none of those models could explain the statistically sharp drop in the m exponents at the $m = 2\mu$ values that were experimentally observed in

both the 2D-like and the 3D-like pore systems that were described in Secs. II and III B. *In short, in contrast to all previous models, we found here that the* $\langle r_i\rangle/\langle r_f\rangle \gg 1$ *feature is a necessary condition for the confinements of the m values, and that the* $\phi_c \to 0$ *feature is a necessary condition for the observation of those confinements.* We have further shown (in Secs. II and III B) that these two necessary conditions are fulfilled in fracture formations and sedimentary rocks.

Not less important is the fact that none of the many previous models that accounted for some particular m values, was based on a simple statistical physics model that recognizes the fact that *Archie's law represents a bona fide phase transition.* This recognition here is based on the fact that only such a percolation phase transition that yields universal exponents can provide a general framework for the understanding of the $\phi_c \to 0$ and the m-confinement features of Archie's law in numerous porous media. This is in spite of the possible richness of, and the differences [54] between, their structural and physical details. Hence, in contrast to all the previous suggestions, our present interpretation and conclusions rely exclusively on statistical physics, via the application of the theory of continuum percolation and its extension by our concept of electrically affected connectivity. Indeed, the fact that the m-values confinement that is found in the above numerous porous media is also found for the electrical conductivity exponent in composite materials [71,119,120] provides convincing evidence that our approach is well justified physically. This follows our observation that, while the electrical conduction mechanism is very different in the two types of systems, the topology of their electrical network is much the same. The above considerations lead us then to provide here the basics for understanding the 78 years old puzzle of Archie's law. These basics are as follows. First, for the systems discussed in the present work the *coupling* of the $r_i \gg r_f$ and the necessary $\phi_c \to 0$ conditions accounts for the $\sigma(\phi)$ dependence of Archie's law and the $\mu < m \leqslant 2\mu$ confinement. This confirms that our solution to Archie's puzzle is holistic. Second, the fact that the only requirement for the observation of Archie's law is the simultaneous fulfillment of these two global conditions explains the abundance of observations in which the Archie's-law behavior has been found. Third, while our holistic solution is a result of the well-based phase transition nature of percolation theory, it also responds to the fundamental request of the pioneering work of Sen *et al.* [54] that "different geometric models must be used for different classes." It is important to note, however, that this is done here within the framework of percolation theory rather than relying on the commonly suggested empirical or ad hoc models. Fourth, in contrast to the doubts [77] regarding the relation of the findings in numerous porous media and the percolation critical behavior, we were able to show (in Sec. III D and Appendix A) that the fact that these findings were derived on a large $(\phi - \phi_c)/\phi_c$ range is the reason, rather than the obstacle, to consider them reliable. In this work, we finally meet the previously unsolved challenge of connecting the m values with the global r_i/r_f and ϕ_{ec} parameters of the studied systems. In particular, we have shown, as confirmed by related simulation studies [22,92], that the "vertical" $m(r_i/r_f)$ transition that was described in relation to Fig. 6 can provide microstructure information on the W/ε ratio in fracture formations and on the $\langle b_v\rangle/\langle\varepsilon\rangle$ ratio in sedimentary rocks.

Following the above we can conclude that while, indeed, the value of m may be a result of a "variety of factors" [38], *what Archie's law actually tells us is that in systems where* $\phi_c \to 0$*, the effect of all those factors culminates in two global and well-defined statistical averages of physical parameters. These are the value of* ϕ_{ec} *and the average* $\langle r_i\rangle/\langle r_f\rangle$ *ratio.* We thus suggest that recognition of these two global statistical properties of a system within the framework of percolation theory, rather than the applications of empirical, partial, or weakly founded models, is the key to the understanding of Archie's law and its applications. As a potentially important application of this observation, we mention that it was previously suggested that accurate m values are of economic importance to the petroleum industry [37,51], and thus our suggested understanding of the m values can be very beneficial to hydrology and petroleum engineers [46]. In particular, drawing $m(\phi)$ maps for a series of $\langle r_i\rangle/\langle r_f\rangle$ values can help in deriving information on the structure parameters of the pores and their relevant distribution functions. For example, for sedimentary rocks one can start by considering the $\langle r_i\rangle/\langle r_f\rangle \approx (\langle b_v\rangle/\langle\varepsilon\rangle)^{3/2}$ relation that we presented in Sec. III B and discussed in Sec. III E. Following then the experimentally derived $m(\phi)$ dependence one can follow the variation of the microstructure in a system with the variation of ϕ. Hence, in contrast to previous suggestions [36], the m values can provide such information in a "readily interpretable form." Another possible application can be based on the connection found between the drop in the value of Archie's exponent when an earthquake is approaching, while the global porosity of the corresponding earth region is hardly changed [32]. Following the above, we can now interpret this behavior as due to the decrease of the $\langle r_i\rangle/\langle r_f\rangle$ ratio for a constant ϕ (see Fig. 6) due to the widening of the participating microfractures in the corresponding porous media.

Considering the above, we have to point out however that a variety of m values inside or outside the Archie's confinements predicted in Eqs. (3)–(6) can be due to effects such as those described in SM(3) of Ref. [56]. On the other hand, we note that none of these effects can explain the well-established confinement of the m and t exponents that is bound by the domain between the upper two curves in Fig. 6. In particular, the sharp statistical drops at 2μ (2.6 in 2D and 4.0 in 3D), that were found by the fitting of $\sigma(\phi)$ data to Archie's law [38,54], clearly prove that the presently suggested electrically affected connectivity in porous media (where $\phi_c \to 0$) and in composite materials (where $x_c \to 0$), accounts for the majority of the observed m values. An interesting case, where a clear distinction can be made between our Archie's universal regime and other m-values regimes, is presented by the data given in Ref. [53]. In that study, a clear and sharp transition between the confined $\mu(3D) < m < 2\mu(3D)$ values at the lower porosity regime, and the very high $m(> 2\mu)$ values at the higher porosity regime, was found. According to our interpretation, this variation of the m values between the two regimes is due to the change of the pores' structure, from being dominated by narrow throats to being dominated by nonslender pores, upon a large increase of the porosity. Indeed, this interpretation is confirmed by the findings in Ref. [53] that the pores' structure

at the higher porosities "is not similar to sedimentary rocks." This sharp transition is then an illustrative confirmation of our holistic statistical phase transition explanation of Archie's law.

V. CONCLUSIONS

The first realization of the present work is that two features characterize Archie's law: the very small percolation threshold ϕ_c, and the statistically determined confinement of the conductivity exponent m within the $\mu \leqslant m \leqslant 2\mu$ interval, where μ is its percolation universal value. The second realization is that in principle, two types of electrical conductivity behaviors can take place in the critical regime of percolation in general, and in porous media with a low-porosity ϕ in particular. If the resistance r_f of the conducting elements, such as brine-filled pores, is larger than the resistance of their connections, such as intersections or throat pores, r_i, Archie's m exponent is determined only by the classical percolation connectivity which is manifested by $m = \mu$. In the opposite, $r_i \gg r_f$, case, the $m(\phi)$ values are confined to the $\mu < m \leqslant 2\mu$ interval. The third realization of the present work is that the necessary condition for the ability to observe such $m \geqslant \mu$ values is a relatively wide critical ϕ regime, prior to the domination of the effective medium behavior. The fourth realization is that this condition can be met by the $\phi_c \to 0$ feature, and that the effect of this feature can be further enhanced, for slender (high aspect ratio) pores, if $r_i \gg r_f$. *In particular, we have shown that these two $\phi_c \to 0$ and $r_i \gg r_f$ conditions, necessary for the observation of the confined m values, are fulfilled by geological fracture formations and channel farms, as well as by sedimentary rocks.* Our conclusion that the observation of the second feature of Archie's law, i.e., the m confinement, depends on the presence of the first feature of this law, i.e., the very small ϕ_c value, couples the two features. This makes *our solution to the puzzle of Archie's law a holistic one.*

The "conceptual" importance of the present work is that it is not based on an empirical, limited, ad hoc, or experiential model, but rather that all its conclusions are derived within the well-established framework of the classical percolation theory as a phase transition. This is in sharp contrast to many past and present evaluations that suggested a lack of a physical and/or first-principles basis for Archie's law. In fact, we have added here a general concept to continuum percolation theory by noting that the critical behavior associated with a particular dynamic property (here, the electrical conductivity) is determined not only by the global geometry of the system (as in the classical percolation theory), but also by the connectivity induced due to that particular property. Being concerned in the present work with electrical conductivity, we called the corresponding phenomenon an electrically affected connectivity. Another general physical conclusion that emerges from the analysis of this work is that a confinement of the critical electrical conductivity exponent as such requires not just a bimodal distribution of the resistors, but that these will be correlated (as $n_i \propto n_f^2$ in the present study). Throughout this work we noted that the same conclusion applies to composite materials of slender conducting particles, thus establishing that all our conclusions stand on a general and firm theoretical basis.

The practical importance of this work is its suggestion that there are two general, statistically culminated parameters on which the evaluation of the observed m values should focus. These parameters are the extrapolated effective medium threshold, ϕ_{ec}, and the global $\langle r_i \rangle / \langle r_f \rangle$ ratio. We thus recommend that when an Archie's law-like behavior is observed, the understanding of the m values that are found should be derived by the calculation or simulation of these two parameters in the corresponding system. In particular, we suggest that this approach can provide information about the microscopic structural and/or physical details of a system by using the $\langle r_i \rangle / \langle r_f \rangle$ values from the experimentally derived $m(\phi)$ values.

Following the above, we can finally conclude that *Archie's law should be taken for what it is, a result of a percolation phase transition with an electrically affected connectivity.* The percolation transition is manifested by the fact that Archie's m values are confined to the μ to 2μ interval, where μ is the percolation universal-critical exponent, and the electrically affected conductivity is manifested by the particular m value that is observed within the above interval. Hence, the power-law expression of Archie's law is not accidental, and neither is the fact that the statistically proven majority of the observed m values is within the above confined m interval. This is not due to effects that are out of the framework of the critical universal behavior that is predicted by percolation theory. Last but not least, we can conclude that for porous media with very low ϕ_c values and high interpore connection resistances, the $m(\phi)$ dependence of the electrical conductivity is determined as follows. At very small ϕ values, m is dominated by the geometrical connectivity of the network and thus $m = \mu$. At intermediate ϕ values, m is also determined by the physical (here, the electrical) connectivity of the network, and thus the m values are confined between μ and 2μ. At still higher ϕ values, m is dominated by the effective medium nature of the system, and thus $m = u \equiv 1$.

ACKNOWLEDGMENTS

The author is indebted to O. Ashkenazy, R. T. DeBold, A. Drory, Y. Goldstein, J. Jedrzejewski, and N. Wagner for many helpful discussions.

APPENDIX A: OBSERVATION OF PERCOLATION CRITICAL BEHAVIOR IN POROUS MEDIA OF SMALL PERCOLATION THRESHOLDS

The observation of the m values in the $\mu < m < 2\mu$ interval in porous media, for the $r_i \gg r_f$ case [see Eq. (4)], is enabled by two effects. The main one is the abundant $\phi_c \to 0$ feature (see Secs. II and III B), and the other (that is described in Appendix B) is the bypassing effect that is associated with slender pores. In Sec. III D we suggested that, in general, the relevant quantity that represents amenably the "width" of the critical regime in percolation, i.e., the regime where the NLB model applies and the μ values are observed, is not $\phi - \phi_c$, but rather $(\phi - \phi_c)/\phi_c$ [72,100]. To illustrate intuitively the justification for this suggestion let us consider a simple comparison of two systems, one in which $\phi_c = 0.01$ and another in which $\phi_c = 0.21$. Now, let us assume a porosity $\phi = 0.22$ in the first system and a porosity $\phi = 0.42$ in the second. In

both systems $\phi - \phi_c = 0.21$. However, it is obvious that the change of the connectivity (i.e., the density of the network; see the NLB in SM(2) of Ref. [56]) between said ϕ_c and ϕ is very different in the two systems. This is because the connectivity change, when ϕ is varied in the $0.01 \leqslant \phi \leqslant 0.22$ range in the system of the lower ϕ_c, is much larger than the change when ϕ is varied in the $0.21 \leqslant \phi \leqslant 0.42$ range in the system of the higher ϕ_c. Recalling that critical behavior is associated with the divergence of the connectivity [74], one would like to have a scale that, when ϕ departs from ϕ_c, is more "representative" than the common $\phi - \phi_c$ scale. Considering then that the only globally available parameter that is associated with the topological connectivity is ϕ_c [82], the only possible amenable measure of the relation between the connectivity and the proximity of ϕ to ϕ_c is the normalized parameter $(\phi - \phi_c)/\phi_c$. This is demonstrated well in our above example where the $(\phi - \phi_c)/\phi_c$ parameter yields $0.21/0.01 \gg 0.21/0.21$, in accordance with the expected much larger connectivity change in the case of the lower ϕ_c. The corresponding general conclusion has been rigorously derived in Ref. [121].

Following the above, let us define the critical regime as the regime where the effect of the connectivity variation on the global conductivity, with the increase of ϕ, is much larger than the EM effect of the variation of the average local conductance (see Sec. III D). Correspondingly, we define the ϕ value at which the transition between the connectivity (percolation)-dominated regime and the regime where the EM effect becomes significant as $\phi_{\rm pec}$. This $\phi_{\rm pec}$ is obviously somewhere in the $\phi_c < \phi < \phi_{ec}$ range, where $\phi_{\rm ec}$ is the extrapolated threshold of the EM-dominated regime. Empirically, this intermediate $\phi_{\rm pec}$ (or $x_{\rm pec}$) can be defined as follows. As already mentioned in Sec. III D the transition from the percolation to the EM regime is accompanied by the reduction of the conductivity critical exponent m (or t) from μ to $u \equiv 1$. Hence, for illustration, an appropriate width of critical range can be defined by $\phi_{\rm pec} - \phi_{\rm c}$ (or $x_{\rm pec} - x_{\rm c}$) where the $\phi_{\rm pec}$ (or $x_{\rm pec}$, or the corresponding $n_{\rm pec}$) that we use is the ϕ (or x, or $n_{\rm f}$) value at which m (or t) becomes $(\mu + u)/2$. We expect then that for a given $\phi_{\rm ec}$ value, the smaller the $\phi_{\rm c}$ the larger the $(\phi_{ec} - \phi_c)/\phi_c$ value, i.e., the larger the connectivity effect, in comparison to the constant-independent EM effect. In other words, the $\phi_{\rm pec}$ ($x_{\rm pec}$) value will shift towards a higher ϕ (or x). The important conclusion is then that this will be manifested by an extended $(\phi - \phi_c)/\phi_c$ [or $(x - x_c)/x_c$] regime, in which the $\mu > (\mu + u)/2$ values will be observed. Effectively, this also means an extended critical regime. Here we remark that the deeper physical reason for this extension of the critical regime when $\phi_c \to 0$ (or $x_c \to 0$) becomes apparent from the known [74,75] NLB picture that is described in SM(2) of Ref. [56]. The smaller the $\phi_{\rm c}$ (or $x_{\rm c}$) the more dilute the "initial" system, and thus the NLB picture will be maintained for larger ϕ (or x) values as ϕ departs from $\phi_{\rm c}$.

Following the above, and recalling the common $\phi_c \to 0$ feature of Archie's porous media [3], and the $x_c \to 0$ feature in many composite materials of slender particles (such as of CNTs, nanowires, or graphene polymer composites [73]), we would expect relatively large $(\phi - \phi_c)/\phi_c$ or $(x - x_c)/x_c$ ranges in which the conductivity exponent will have the universal value of μ. Indeed, there are numerous examples of systems with low percolation thresholds where the percolation critical behavior is manifested by $m = \mu$ or $t = \mu$ observations over very large $(\phi - \phi_c)/\phi_c$ ranges (as high as 20 [2,19,54]) or $(x - x_c)/x_c$ ranges (as high as 100 [98,107,122–124]). We remark here in passing that, as noted at the end of Sec. III C, our present conclusions and the cited experimental confirmations are contrary to the *a priori* intuitive conclusions, such as that of Feng *et al.* in Ref. [77]. They suggested that: "Experiments on rocks, however, are typically made in the regime $(\phi - \phi_c)/\phi_c > 1$, so we have no right, a priori, to expect that asymptotic critical exponents will apply." Our present analysis shows that for $\phi_c \to 0$ there is an extension of the critical regime, and thus that we are right in considering the $\mu \leqslant m \leqslant 2\mu$ values that were derived on numerous porous media, as reflecting the critical behavior of percolation. Of particular importance to our argument in Sec. III D are the systematic findings of Ref. [79] that in conducting porous media of low porosity, such as sandstones, the typical corresponding ϕ_{ec}/ϕ_c ratio is within the 30–40 range, and that there is no apparent dependence of $\phi_{\rm ec}$ on $\phi_{\rm c}$. *Hence, the basic condition for the ability to observe the m values in the confined $\mu \leqslant m \leqslant 2\mu$ interval is fulfilled in both types of porous media that are considered in the present work.*

Finally, in accordance with the above conclusion that is also manifested in Fig. 6, one finds that in all the works where the $m(\phi)$ or the $t(x)$ values were studied over wide $(\phi - \phi_c)/\phi_c$ or $(x - x_c)/x_c$ ranges [38,119,124–127], these values were found to be confined to the μ-2μ interval. Moreover, the finding of the same m and t dependencies in simulations of 2D line segments [86,92] and small void-pore [22] systems, suggests that the corresponding ability to observe the m-values confinement is due to the common low-percolation threshold [3,73] in all those systems. The fact that the results of these simulations are representative of both types of porous media that are of interest in the present work, as well as for composites of slender particles, indicates that indeed it is the low-percolation threshold that enables the observation of the $\langle r_i \rangle \gg \langle r_f \rangle$ induced $m > \mu$ and $t > \mu$ values in all those systems.

APPENDIX B: EXPANSION OF THE CONDUCTIVITY CRITICAL REGIME DUE TO SLENDER PORES WITH A LARGE $r_{\rm i}/r_{\rm f}$ RATIO

To understand this effect let us reconsider the percolation and EM regimes (see Sec. III D), but with a special emphasis on the vicinity of the transition between them, by following the effect of an additional conducting element on the $m(n_{\rm f})$ dependence. In the percolation regime (see SM(2) in Ref. [56]), the main role of such an addition is to initiate a local or nonlocal conducting path, while in the EM regime it is to be attached in parallel to an element, such as a singly connected bond (SCB) or a blob of the existing dense conducting network [109]. The resulting effect in the EM regime will be then to increase slightly the average local conductance of a link without changing the topology of the network. For the vicinity of the transition between the two regimes, we can assume that the basic structure of the backbone is still maintained, except that the links are somewhat shorter and the blobs are somewhat larger and denser than in the percolation regime (see SM(2) in Ref. [56]). In the classical-lattice theories the

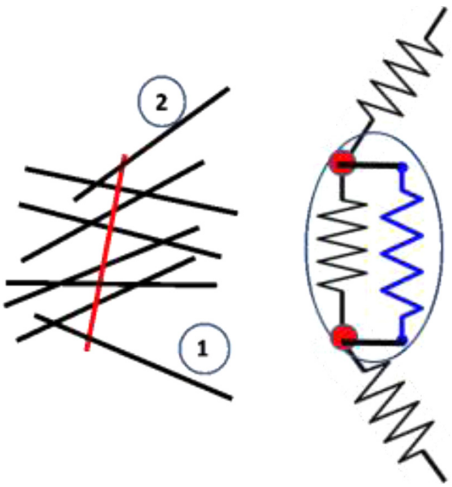

FIG. 7. An illustration of the geometrical (left) and the corresponding electrical part of a link (right) where a (red) slender low-resistance stick bypasses an existing high-resistance blob at the vicinity of the percolation to EM transition. The corresponding single added (black) resistor "shortens" the (blue) parallel resistance of the blob and effectively turns the resistance of their combination to that of the added stick.

percolation to EM transition [38,96,109] is manifested by the decrease of m from $m = \mu$ to $m = u \equiv 1$ (see Appendix A).

Turning to the continuum, let us assume that the conducting objects are permeable circles. In that case, the network will be similar to that of a lattice [112] and an added circle can only be connected in parallel to a single, or at most to two neighboring circles. The size of the added conducting object (or bond) is then practically the same as that of a single circle component of an existing blob. Correspondingly, the geometrical and electrical outcomes of the added circle will be the same as in the case of an added bond in a lattice, where the lattice is above the percolation threshold. Now let us consider the resulting behavior when the conducting objects are the slender line-segment sticks of length L, such as in Fig. 1. At the percolation end of the percolation to EM transition, the blobs will be generally somewhat shorter (and denser) than in the percolation regime, but they will generally be longer than at the EM end of that transition regime. As illustrated in Fig. 7, under these conditions there are blobs that are shorter than L. In that illustration, the added (red) stick is connected in parallel to the blob of line-segment sticks between the SCB (1) and the SCB (2). From the electrical point of view the system is equivalent then to a series connection of three resistors, where the central one is a parallel combination of the added (black) resistor and the resultant (blue) resistor of the blob prior to this addition. This yields, of course, a lower resistance than that of the original blob. Suppose now that the resistance of the added slender object $r_{\rm f}$, is "somehow" much smaller than that of the original blob, the added resistor can then (closely) replace the combined parallel combination yielding an equivalent series system of the resulting three SCBs. Here, in contrast with the case of the classical NLB model (see SM(2) in Ref. [56]), the much higher resistance of the blob in comparison with $r_{\rm f}$, is possible, if the resistance $r_{\rm i}$ of the intersections between two sticks in the blob is much larger than the resistance of the sticks themselves. The blob, in the left of Fig. 7, illustrates such a situation where prior to the addition of the new stick, the blob connecting the SCBs (1) and (2) involves some necessary $r_{\rm i}$s. Of course, due to the (red dot) interconnection between the blobs and SCBs, or between SCBs, the overall conductivity will still be proportional to $1/r_{\rm i}$ but it will be higher than the one prior to the addition of the parallel $r_{\rm i}$. Such an addition of the conducting sticks in the EM vicinity of the transition will be then to increase the conductivity of the electrical network, as well as to make the links to consist of more low-resistance SCBs, at the "expense" of the original high-resistance blobs. The higher the $r_{\rm i}/r_{\rm f}$ ratio, the more pronounced those effects.

Turning to the implications of the above SCB-like geometrical bypassing of the $r_{\rm i}$-dominated blobs in a link, by the added low-resistance sticks, let us recall the well-established statistics of the backbone in percolation theory. In particular, the probability of a given bond in the system (say, a resistor $r_{\rm f}$) to belong to the backbone is given by $P_B(n_{\rm f}) \propto (n_{\rm f} - n_{\rm fc})^{\beta B}$, where $\beta B(2{\rm D}) \approx 0.5$ and $\beta B(3{\rm D}) \approx 1.0$ [76,128–130]. We also recall that the probability of being a singly connected bond within the backbone diverges when $n_f \to n_{fc}$, as expressed by the $L_1 \propto (n_f - n_{fc})^{-1}$ relation that is given in SM(2) of Ref. [56]. This means that when $n_{\rm f}$ decreases towards $n_{\rm fc}$, there is a relatively strong increase in the number of the SCBs in comparison with all other bonds in the backbone [76]. This is also expected intuitively since the decrease of $n_{\rm f}$ towards $n_{\rm fc}$ causes the links of the backbone to become longer and the blobs in them to become "slimmer," due to the loss of "superfluous" blob's related bonds.

Returning to the above bypassing of parts of the link by single slender objects, we note now the topological similarity between the above increase of the SCB nature of the links by the addition of slender objects, and the general relative increase of the relative SCBs concentration when the percolation threshold is approached. Hence, for the very same geometrical network of resistors, the one with the larger $r_{\rm i}/r_{\rm f}$ ratio will yield a network that, from the electrical conductivity point of view, is effectively "deeper" in the critical regime due to the resulting increase of the number of SCBs in a link. Consequently, the result of the parallel connection of an added slender low-resistance stick is not only to increase the local conductivity of some parts of the system [99], but no less importantly to electrically take the system from being at the edge of the onset of the EM regime to behave as if it belongs to the critical regime

To check the validity of the above argument, let us examine first the expected manifestation of our latter conclusion within the framework of the behavior that we predicted in Fig. 6. In the analysis given in Sec. III E, we predicted that for the $r_i \gg r_f$ case the increase of $n_{\rm f}$ (or ϕ) will be accompanied by the increase of m from μ, up to 2μ. Then, with a further increase of $n_{\rm f}$ (or ϕ) due to the approach to the EM regime, there will be a decrease of m from its peak value towards the $u \equiv 1$ value. Correspondingly, we predicted that the $m(n_{\rm f})$ dependence will have a maximum value within the $\mu \leqslant m \leqslant 2\mu$ interval, and that this maximum will be obtained at some $n_f = n_{fm}$. We also predicted that the larger the $r_{\rm i}/r_{\rm f}$ ratio, the higher the value of m would be at this $n_{\rm fm}$. Here we add a new prediction, i.e., that with the increase of this ratio the larger will be the effect of the parallel additions, i.e., there will be an expansion of the

critical percolation regime at the "expense" of the EM regime. The effect of this is expected to be manifested by a shift of $n_{\rm fm}$ towards larger $n_{\rm f}$ value. Combining the latter two conclusions, we finally predict that the increase of $r_{\rm i}/r_{\rm f}$ will simultaneously cause an increase in the value of m and the shift of $n_{\rm fm}$ to larger $n_{\rm f}$ values. This prediction is well exhibited by the $n_{\rm fm}$ shift that was observed in the simulation results of Zezelj and Stankovic [92], but has not been discussed by them.

We can summarize now that in systems of slender conducting objects, both the $\phi_e \to 0$ feature (see Sec. II and Appendix A) and the $r_{\rm i}/r_{\rm f}$ ratio determine the width of the effective percolation critical regime of the electrical conductivity. As far as we know, neither of these predictions, and clearly not their combination, has been reported previously. Finally, we remark that there is a general physical importance to the above conclusion. This is the finding that the effective critical regime for a given dynamical property depends not only on the geometrical structure of the system, but also on the particular characteristics of this (here the electrical) property.

[1] G. E. Archie, The electrical resistivity log as an aid in determining some reservoir characteristics, Trans. AIME (Am. Inst. Min. Metallurgy) Pet. Eng. **46**, 54 (1942).

[2] A. Hunt, R. Ewing, and B. Ghanbarian, *Percolation Theory for Flow in Porous Media* (Springer, Cham, 2014).

[3] I. Balberg, Excluded-volume explanation of Archie's law, Phys. Rev. B **33**, 3618 (1986).

[4] M. S. Paterson, The equivalent channel model for permeability and resistivity in fluid-saturated rock—a re-appraisal, Mech. Mater. **2**, 345 (1983).

[5] B. Kozlov, M. H. Schneider, B. Montaron, M. Lagues, and P. Tabeling, Archie's law in microstructures, Transp. Porous Media **95**, 1 (2012).

[6] D. Roubinet, J. Irving, and P. A. Pezard, Relating topological and electrical properties of fractured porous media: Insights into the characterization of rock fracturing, Minerals **8**, 14 (2018).

[7] Y. Liu and P. K. Kitasides, in *Tortuosity and Archie's Law, Advances in Hydrology*, edited by M. K. Phoolendra and K. L. Kristopher (Springer, New York, 2013), Chap. 6.

[8] M. Kuntz, J. C. Mareschal, and P. Lavall'ee, Numerical estimation of electrical conductivity in saturated porous media with 2-D lattice gas, Geophysics **65**, 766 (2000).

[9] S. A. Trugman and A. Weinrib, Percolation with a threshold at zero: A new universality class, Phys. Rev. B **31**, 2974 (1985).

[10] Z. Liu, J. E. McClure, and T. Armstrong, Influence of wettability on phase connectivity and electrical resistivity, Phys. Rev. E **98**, 043102 (2018).

[11] Q. Niu and C. Zhang, Physical Explanation of Archie's Porosity Exponent in Granular Materials: A Process-Based Pore-Scale Numerical Study, Geophys. Res. Lett. **45**, 1870 (2018)).

[12] P-Z. Wong, The statistical physics of sedimentary rocks, Phys. Today **41**(12), 24 (1988).

[13] R. He, H. Ma, R. B. Hafiz, C. Fu, X. Jin, and J. He, Determining porosity and pore network connectivity of cement-based materials by a modified non-contact electrical resistivity measurements: Experiment and theory, Mater. Des. **156**, 82 (2019).

[14] X. Zhu, Z. Zhang, K. Yang, B. Magee, Y. Wang, L. Yu, S. Nanukuttan, Q. Li, S. Mu, C. Yang, and M. Basheer, Characterization of pore structure development of alkali-activating slag cement during early hydration using electrical responses, Cem. Concr. Compos. **89**, 139 (2018).

[15] A. Cordier, H. El Khal, E. Siebert, and M. C. Stell, On the role of pore morphology on the electrical conductivity of porous yttria-stabilized zirconia, J. Eur. Ceram. Soc. **39**, 2518 (2019).

[16] K. Li, M. Qin, and Q. Gui, Durability properties of structural concretes containing secondary cementitious materials, Green Mater. **7**, 40 (2019).

[17] M. Rangelov and S. Nssiri, Empirical time-dependent tortuosity relations for hydrating mortar mixtures based on modified Archie's law, Constr. Build. Mater. **171**, 825 (2018).

[18] M.-C. Bay, M. V. F. Heinz, R. Figi, C. Schreiner, D. Basso, N. Zanon, U. F. Vogt, and C. Battaglia, Impact of liquid phase formation on microstructure and conductivity of Li-stabilized Na-β"–alumina ceramics, ACS Appl. Energy Mater. **2**, 687 (2019).

[19] S. P. Friedman, Soil properties influencing apparent electrical conductivity: A review, Comput. Electron. Agric. **46**, 45 (2005).

[20] Q. Sun and C. Lu, Semi-empirical correlation between thermal conductivity and electrical resistivity for silt and silty clay soils, Geophysics **84**, MR99 (2019).

[21] T. Herring, E. Cey, and A. Pidlisecky, Electrical resistivity of partially saturated porous media at subzero temperatures, Vadose Zone J. **18**, 190019 (2019).

[22] W. Feng, W. Zhu, Y. Cong, W. Xianhu, X. Yaping, and C. Linlin, Numerical simulation of the influence of pore structure on resistivity, formation factor and cementation index in tight sandstone, Acta Geol. Sin. (Engl. Ed.) **94**, 290 (2020).

[23] M. J. Stephens, D. H. Shimabukuro, J. M. Gillespie, and W. Chang, Groundwater salinity mapping using geophysical log analysis within the Fruitvale and Rosedale Ranch oil fields, Kern County, California, USA, Hydrology J. **27**, 731 (2019).

[24] N. Brindt, M. Rahav, and R. Wallach, ERT and salinity-a method to determine whether ERT-detected preferential pathways in brackish water-irrigated soils are water-induced or an artifact of salinity, J. Hydrol. **574**, 35 (2019).

[25] J. Dick, D. Tetzlaff, J. Bradford, and C. Soulsby, Using repeat electrical resistivity surveys to assess heterogeneity in soil moisture dynamics under contrasting vegetation types, J. Hydrol. **559**, 684 (2018).

[26] Y. Han, C. Zhou, J. Yu, and C. Li, Experimental investigation on the effect of wettability on rock-electricity responses in sandstone reservoirs, Fuel **239**, 1246 (2019).

[27] W. Zairani, W. Bakar, I. M. Saaid, M. R Ahmad, Z. Amir, and S. Q. Mahat, Derivation of formation factor in shaly sandstone with geometry and clay conductivity effects, J. Pet. Sci. Eng. **182**, 106359 (2019).

[28] G. Spagnoli, B. A. Weymer, M. Jegen, E. Spangenberg, and S. Petersen, P-wave velocity measurements for preliminary assessments, of the mineralization in seafloor massive sulfide mini-cores during drilling operations, Eng. Geol. **226**, 316 (2017).

[29] R. Monroy and M. W. John, Monitoring the electrical properties of metal ore mine tailings during sedimentation, Environ. Geotech. **6**, 146 (2019).

[30] A. Revil, M. Le Breton, Q. Niu, E. Wallin, E. Haskins, and D. M. Thomas, Induced polarization of volcanic rocks-1. Surface versus quadrature conductivity, Geophys. J. Int. **208**, 826 (2017).

[31] KH. Imomnazarov, Archie's law for a mathematical model of movement of a conducting liquid through a conducting porous medium, Appl. Math. Lett. **11**, 135 (1998).

[32] M. Merzer and S. L. Klemperer, Modeling low-frequency magnetic-field precursors to the Loma Prieta earthquake with a precursory increase in fault-zone conductivity, Pure Appl. Geol. **150**, 217 (1998).

[33] J. Hu, X. W. Wu, H. Ke, X. B. Xu, J. W. Lan, and L-t. Zhan, Application of electrical resistivity tomography to monitor the dewatering of vertical and horizontal wells in municipal solid waste landfills, Eng. Geol. **254**, 1 (2019).

[34] A. C. Knight, A. D. Werner, and D. J. Irvine, Combined geophysical and analytical methods to estimate offshore freshwater extent, J. Hydrol. **576**, 529 (2019).

[35] L-t. Zhan, H. Xu, X-m. Jiang, J-w. Lan, Y-m. Chen, and Z-y. Zhang, Use of electrical resistivity tomography for detecting the distribution of leachate and gas in large scale MSW landfill cell, Environ. Sci. Pollut. Res. **26**, 20325 (2019).

[36] D. W. Kennedy and D. C. Herrick, Conductivity models for Archie's rocks, Geophysics **77**, WA109 (2012).

[37] B. Montaron, Connectivity theory-a new approach to modeling non-Archie rocks, Petrophysics **50**, 102 (2009).

[38] M. Sahimi, *Heterogeneous Materials, I. Linear Transport and Optical Properties* (Springer, New York, 2003).

[39] J. Cai, W. Wei, X. Hu, and D. A. Wood, Electrical conductivity models in saturated porous media: A review, Earth Sci. Rev. **171**, 419 (2017).

[40] H. Dashtian, Y. Yang, and M. Sahimi, Nonuniversality of the Archie exponent due to multifractality of resistivity well logs, Geophys. Res. Lett. **42**, 10655 (2015).

[41] A. J. Katz and A. H. Thomson, Fractal Sandstone Pores: Implications for Conductivity and Pore Formation, Phys. Rev. Lett. **54**, 1325 (1985).

[42] M. Jonas, J. R. Schopper, and J. H. Schon, Mathematical-physical reappraisal of Archie's first equation on the basis of a statistical network model, Transp. Porous Media **40**, 243 (2000).

[43] O. A. L. de Lima and M. M. Sharma, A grain conductivity approach to shaly sandstones, Geophysics **55**, 1347 (1990).

[44] A. De Kuijper, A. Sandor, J. P. Hofman, and J. A. De Wall, Conductivity of two-component systems, Geophysics **61**, 162 (1996).

[45] R. Freedman, Moving beyond Archie's legacy in the 21st century, Petrophysics **51**, 468 (2009).

[46] R. C. Ransom, Moving beyond Archie's legacy in the 21st century: Reply, Petrophysics **51**, 12 (2010).

[47] W. Yue, Pore-scale explanation of the Archie's cementation exponent: Microstructure, electrical anisotropy, and numerical experiments, Geophys. Res. Lett. **46**, 5799 (2019).

[48] H. Wang and T. Liu, Derivation of Archie's law based on a fractal pore volume, Geophys. J. Int. **209**, 1403 (2017).

[49] H. Meng, Study of the rock-electric and the relative permeability characteristics in porous rocks based on the curved cylinder-spherical model, J. Pet. Sci. Eng. **166**, 891 (2018).

[50] Z. Tariq, M. Mahmoud, H. Al-Youssef, and M. R. Kahn, Carbonate rocks resistivity determination using dual and triple porosity conductivity models, Petroleum **6**, 35 (2019).

[51] P. W. Glover, A new theoretical interpretation of Archie's saturation exponent, Solid Earth **8**, 805 (2017).

[52] L. D. Thanh, D. Jougnot, P. Van Do, and N. Van Nghia, A physically based model for the electrical conductivity of water-saturated porous media, Geophys. J. Int. **219**, 866 (2019).

[53] H. M. N. Wright, K. V. Cashman, E. H. Gottesfeld, and J. R. Roberts, Pore structure of volcanic clasts: Measurements of permeability and electrical conductivity, Earth Planet. Sci. Lett. **280**, 93 (2009).

[54] P. N. Sen, C. Scala, and M. H Cohen, A self-similar model for sedimentary rocks with application to the dielectric constant of fused glass-beads, Geophysics **46**, 781 (1981).

[55] P. D. Chinh, Electrical properties of sedimentary rocks having interconnected water-saturated pore spaces, Geophysics **65**, 1093 (2000).

[56] See Supplemental Material at http://link.aps.org/supplemental/10.1103/PhysRevE.103.063005 for various data on the conductivity critical exponents in porous media and composite materials, and a brief review of the classical theory of these exponents within the framework of universal and nonuniversal percolation [57–69].

[57] L. Wang, Z. Mao, Y. Shi, Q. Tao, Y. Cheng, and Y. Song, A novel model for predicting Archie's cementation factor from nuclear magnetic resonance (NMR) logs in low permeability reservoirs, J. Earth Sci. **25**, 183 (2014).

[58] N. Neithalath, J. Weiss, and J. Olek, Characterizing enhanced porosity concrete using electrical impedance to predict acoustic and hydraulic performance, Cem. Concr. Resour. **36**, 2074 (2006).

[59] P. D. Jackson, D. Taylor Smith, and P.N. Stanford, Resistivity-porosity-particle shape relationship for marine sands, Geophysics **43**, 1250 (1978).

[60] M. R. J. Wyllie and A. R. Gregory, Fluid flow through unconsolidated porous aggregates: Effect of porosity and particle shape on Kozeny-Carmen constants, Ind. Eng. Chem. **47**, 1379 (1955).

[61] R. Zallen, *The Physics of Amorphous Solids* (John Wiley & Sons, New York, 1983).

[62] M. B. Bryning, M. F. Islam, J. M. Kikkawa, and A. G. Yodh, Very low conductivity Threshold in bulk isotropic single-walled carbon nanotube-epoxy composites, Adv. Mater. **17**, 1186 (2005).

[63] K. Ahmad, W. Pan, and S. L. Shi, Electrical conductivity and dielectric properties of multiwalled carbon nanotube and alumina composites, J. Appl. Phys. **89**, 133122 (2006).

[64] P. D. Chinh, Modeling the conductivity of highly consolidated, bi-consolidated porous rocks, J. Appl. Phys. **84**, 796 (1998).

[65] I. Balberg, The tunneling percolation problem, J. Phys. D: Appl. Phys. **42**, 064003 (2009).

[66] C. J. Lobb, D. J. Frank, and M. Tinkham, Percolative conduction in anisotropic media: A Renormalization-Group approach, Phys. Rev. B **23**, 2262 (1981).
[67] J. F. McCarthy, Continuum Percolation of Disks and the Random Lattice, Phys. Rev. Lett. **58**, 2242 (1987).
[68] O. Stenwell and H-K. Janssen, Conductivity of continuum percolation systems, Phys. Rev. E **64**, 056105 (2001).
[69] I. Balberg and N. Binenbaum, Cluster structure and conductivity of three-dimensional continuum systems, Phys. Rev. A **31**, 1222 (1985).
[70] J. N. Roberts and L. M. Schwartz, Grain consolidation and electrical conductivity in porous media, Phys. Rev. B **31**, 5990 (1985).
[71] W. Bauhofer and J. Z. Kovacs, A review and analysis of electrical percolation in carbon nanotube polymer composites, Compos. Sci. Technol. **69**, 1486 (2009).
[72] R. M. Mutiso and K. I. Winey, Electrical percolation in quasi-two-dimensional metal nanowire networks for transparent conductors, Phys. Rev. E **88**, 032134 (2013).
[73] I. Balberg, The importance of bendability in the percolation behavior of carbon nanotube and graphene-polymer composites, J. Appl. Phys. **112**, 066104 (2012).
[74] D. Stauffer and A. Aharony, *Introduction to Percolation Theory* (Taylor & Francis, London, 1994).
[75] B. I. Shklovskii and A. L. Efros, *Electronic Properties of Doped Semiconductors* (Springer, Heidelberg, 1984).
[76] A. Bunde and S. Havlin, *Fractals and Disordered Systems* (Springer, New York, 1991).
[77] S. Feng, B. I. Halperin, and P. N. Sen, Transport-properties of continuum systems near the percolation-threshold, Phys. Rev. B **35**, 197 (1987).
[78] I. Balberg, Principles of the theory of continuum percolation, in *Encyclopedia of Complexity and Systems Science*, edited by R. A. Meyers, A. Hunt, and M. Sahimi (Springer, Berlin, 2020).
[79] B. Ghanbarian, A. G. Hunt, R. P. Ewing, and T. E. Skinner, Universal scaling of the formation factor in porous media derived by combining percolation and effective medium theories, Geophys. Res. Lett. **41**, 3884 (2014).
[80] A. Aydin and Z. Reches, Number and orientation of fault sets in the field and the experiments, Geology **10**, 107 (1982).
[81] W. F. Brace, A. S. Orange, and T. R. Madden, The effect of pressure on the electrical resistivity of water-saturated crystalline rocks, J. Geophys. Res. **70**, 5669 (1965).
[82] I. Balberg, C. H. Anderson, S. Alexander, and N. Wagner, Excluded volume and its relation to the onset of percolation, Phys. Rev. B **30**, 3933 (1984).
[83] J. Zhao, X-Y. Dai, Y-F. Lu, and S-H. Tang, Shale reservoir conductive simulation based on percolation networks, Chin. J. Geophys.-Chin. Ed. **60**, 275 (2017).
[84] Y-J. Park, K-K. Lee, and B. Berkowitz, Effects of junction transfer characteristics on transport in fracture networks, Water Resour. Research **37**, 909 (2001).
[85] J. Zaba, Z. Malolepszy, K. Gaidzik, J. Ciesielczuk, and A. Paulo, Fault network in Rio Cola valley between Maca and Pinchollo, Central Andes, Southern Peru, Ann. Soc. Geol. Pol. **82**, 279 (2012).
[86] I. Balberg, N. Binenbaum, and C. H. Anderson, Critical Behavior of the Two-Dimensional Sticks System, Phys. Rev. Lett. **51**, 1605 (1983).
[87] I. Balberg, B. Berkowitz, and G. E. Drachsler, Application of a percolation model to flow in fractured hard rocks, J. Geophys. Res.: Solid Earth Planets **96**, 10015 (1991).
[88] Y. F. Alghalandis, C. Xu, and P. A. Dowd, A general framework for fracture intersection analysis: Algorithms and practical applications, in *Proceeding of the Australian Geothermal Energy Conference*, Vol. 15 (2011).
[89] A. Saieed, W. Pao, and F. M. Hashim, Effect of T-junction diameter ratio on stratified-wavy flow separation, J. Nat. Gas Sci. Eng. **51**, 223 (2018).
[90] N. King Huber, The geologic story of Yosemite National Park, USGS Numbered Series, Bulletin No. 1595 (U.S. Government Printing Office, California, 1987).
[91] I. Balberg, N. Wagner, D. W. Hearn, and J. A. Ventura, Critical Behavior of the Electrical Resistance and Its Noise in Inverted Random-Void Systems, Phys. Rev. Lett. **60**, 1887 (1988).
[92] M. Zezelj and I. Stankovic, From percolation to dense random stick networks: Model investigation, Phys. Rev. B **86**, 134202 (2012).
[93] I. Balberg, D. Azulay, Y. Goldstein, and J. Jedrzejewski, Possible origin of the smaller than universal percolation conductivity exponent in the continuum, Phys. Rev. E **93**, 062132 (2016).
[94] I. Balberg, Universal percolation-Threshold limits in the continuum, Phys. Rev. B **31**, 4053 (1985).
[95] D. Di Naccio, P. Boncio, S. Cirill, F. Casaglia, E. Morettini, G. Lavecchia, and F. Brozzetti, Role of mechanical stratigraphy on fracture development in carbonates reservoir: Insights from outcropping shallow water carbonates in the Umbria-Marche Apennines, Italy, J. Volcanol. Geotherm. Res. **148**, 98 (2012).
[96] C. W. Nan, Physics of inhomogeneous inorganic materials, Prog. Mater. Sci. **37**, 1 (1993).
[97] R. Murphy, V. Nicolosi, Y. Hernandez, D. McCarthy, D. Rickard, D. Vrbanic, A. Merzel, D. Mihailovic, W. J. Blau, and J. N. Coleman, Observation of extremely low percolation threshold in $Mo_6S_{4.5}I_{4.5}$ nanowire/polymer composites, Scr. Mater. **54**, 417 (2006).
[98] M. Foygel, R. D. Morris, D. Anez, S. French, and V. L. Sobolev, Theoretical and computational studies of carbon nanotube composites and suspensions: Electrical and thermal conductivities, Phys. Rev. B. **71**, 104201 (2005).
[99] J. Li and S-L. Zhang, Conductivity exponents in sticks percolation, Phys. Rev. E **81**, 021120 (2010).
[100] P. Keblinski and F. Cleri, Contact resistance in percolating networks, Phys. Rev. B **69**, 184201 (2004).
[101] S. I. Ozkaya and J. Mattner, Fracture connectivity from fracture intersections in borehole image logs, Comput. Geophys. **29**, 143 (2003).
[102] D. Or and T. A. Ghezzehel, Traveling liquid bridges in unsaturated fractured porous media, Transp. Porous. Media **68**, 129 (2007).
[103] W. Shockley, *Electrons and Holes in Semiconductors* (Van Nostrand, Princeton, 1953).
[104] I. Braun and H. K. Henish, Characteristics of injecting point contacts on semiconductors-I In darkness, Solid State Electron. **9**, 981 (1966).
[105] D. C. P. Peacock, V. Dimmen, A. Rotevatn, and D. J. Sanderson, A broader classification of damage zones, J. Struct. Geol. **102**, 179 (2017).

[106] A. N. Kravchenko, G. A. Bollero, R. A. Omonode, and D. G. Bullock, Quantitative mapping of soil drainage classes using topographical data and soil electrical conductivity, Soil Sci. Soc. Am. J. **66**, 235 (2002).

[107] Y. J. Kim, T. S. Shin, H. D. Choi. J.H. Kwon, Y. C. Chung, and H. G. Yoon, Electrical conductivity of chemically modified multiwalled carbon nanotube/epoxy composites, Carbon **43**, 23 (2005).

[108] M. Kashif, Y. Cao, G. Yuan, M. Asif, K. Javed, J. N. Mendez, D. Khan, and L. Miruo, Pore size distribution, their geometry, and connectivity in deeply buried paleogene Es1 sandstone reservoir, Nanpu Sag, East China, Pet. Sci. **16**, 981 (2019).

[109] S. Kirkpatrick, Percolation and conduction, Rev. Mod. Phys. **45**, 574 (1973).

[110] Y. Tang, J. Xu, and J. Zhou, Applicability of cavity-throat connecting model for estimating the hydraulic conductivity of fine-ground soils: A geometrical and mathematical approach, J. Soils Sediments **19**, 652 (2019).

[111] Y. Gueguen, T. Chelideze, and M. Le Ravalec, Microstructures, percolation thresholds and rock physical properties, Tectonophysics **279**, 23 (1997).

[112] H. Scher and R. Zallen, Critical density in percolation processes, J. Chem. Phys. **53**, 3759 (1970).

[113] B Abeles, P. Sheng, M. D. Coutts, and Y Arie, Structural and electrical properties of granular metal films, Adv. Phys. **24**, 407 (1975).

[114] L. Fonseca and I. Balberg, Resistivity and electrical noise in granular metal composites, Phys. Rev. B **48**, 14915 (1993).

[115] P. M. Kogut and J. Straley, Distribution-induced non-universality exponents, J. Phys. C: Solid State Phys. **12**, 2151 (1979).

[116] S. Rafiee, A. Hashemi, and M. Shahi, A new cementation factor correlation in carbonate parts of oil-fields in South-West Iran, Iran. J. Oil Gas Sci. Technol. **3**, 1 (2014).

[117] M. Hassani-giv and M. Rahimi, New correlation for porosity exponent in carbonate reservoirs of Iranian oil fields in Zagros Basin, JSUT (Journal of Science/University of Tehran) **34**, 1 (2008).

[118] A. M. Borai, A new correlation for cementation factor in low-porosity carbonates, SPE Form. Eval. **2**, 495 (1987).

[119] A. Combessis, L. Bayon, and L. Flandin, Effect of filler auto-assembly on percolation transition in carbon nanotube/polymer composites, Appl. Phys. Lett. **102**, 011907 (2013).

[120] S. Rul, F. Lefevre-Schlick, E. Capria, Ch. Laurent, and A. Peigney, Percolation of single-walled carbon nanotubes in ceramic matrix nanocomposites, Acta Mater. **52**, 1061 (2004).

[121] T. Kaliski and R. Cohen, Width of the percolation transition in complex networks, Phys. Rev. E **73**, 035101 (2006).

[122] M. O. Lisunova, Ye. P. Mamunya, N. I. Lebovka, and A. V. Melezhyk, Percolation behavior of ultrahigh molecular weight polyethylene/multi-walled carbon nanotubes composites, Eur. Polym. J. **43**, 949 (2007).

[123] J. M. Benoit, B. Corrazc, and O. Chauvet, Localization, Coulomb interactions, and electrical heating in single-wall carbon nanotubes/polymer composites, Phys. Rev. B **65**, 241405(R) (2002).

[124] A. E. Eken, E. J. Tozzi, D. J. Klineberg, and W. Bauhofer, A simulation study on the combined effects of nanotube shape and shear flow on the electrical percolation Thresholds of carbon nanotube/polymer composites, J. Appl. Phys. **109**, 084342 (2011).

[125] S. Abbasi, P. J. Carreau, and A. Derdouri, Flow induced orientation of multiwalled carbon nanotubes in polycarbonate nanocomposites: Rheology, conductivity and mechanical properties, Polymer **51**, 922 (2010).

[126] S. J. Chin, S. Vempaii, P. Dawson, M. Knite, A. Linarts, K. Ozols, and T. McNally, Electrical conduction and rheological behavior of composites of poly (ε-caprolactone) and MWCNTs, Polymer **58**, 209 (2015).

[127] P. S. Kang and G. T. Kim, Effects of junctions on carbon nanotube network-based devices, Phys. Status Solidi B **248**, 2644 (2011).

[128] M. Sahimi, Scaling relation for the critical exponents of the backbone of percolation clusters, J. Phys. A: Math. Gen. **17**, 3073 (1984).

[129] H. J. Herrmann and H. E. Stanley, Building Blocks of Percolation Clusters: Volatile Fractals, Phys. Rev. Lett. **53**, 1121 (1984).

[130] C. A. Moukarzei, A fast algorithm for backbones, Int. J. Mod. Phys. C **09**, 887 (1998).